EAVN Status Report for the 2020A Semester

EAVN User Support Team, NAOJ, SHAO, XAO, and KASI

October 31, 2019

Additional notification to EAVN proposers (revised on 2019 October 31)

- Available date for EAVN observations with Nobeyama 45-m telescope is fixed from 2019 April 21 through 24. Refer to Section 3.1 (p.26) for more details.
- Table 11 (p.28) was modified.

Major revision since the 2019B semester

• Takahagi 32-m telescope joins in EAVN observations at 22 GHz (see Sections 2.1, 2.2, 2.3, 3.1, 3.4)

Contents

L I	Intr	oducti	on						
2 5	Syst	tem							
4	2.1	Array							
2	2.2	Anten	nas						
		2.2.1	Brief Summary of VERA Antennas						
		2.2.2	Brief Summary of KVN Antennas						
		2.2.3	Nobeyama 45-m Telescope						
		2.2.4	Takahagi 32-m Telescope						
		2.2.5	Tianma 65-m Telescope						
		2.2.6	Nanshan 26-m Telescope						
		2.2.7	Aperture Efficiency						
		2.2.8	Beam Pattern and Size						
4	2.3	Receiv	rers						
		2.3.1	Brief Summary of VERA Receiving System						
		2.3.2	Brief Summary of KVN Receiving System						
		2.3.3	Brief Summary of NRO45 Receiving System						
		2.3.4	Brief Summary of TAK32 Receiving System						
		2.3.5	Brief Summary of TMRT65 Receiving System						
		2.3.6	Brief Summary of NSRT26 Receiving System						
4	2.4	Digita	l Signal Processing						
4	2.5	Record	ders						
4	2.6	Correl	ators						
		2.6.1	Note for the C2 mode						
4	2.7	Calibr	ation						
		2.7.1	Delay and Bandpass Calibration						
		2.7.2	Gain Calibration						
6	2.8	Geode	tic Measurement						
		2.8.1	Brief Summary of VERA Geodetic Measurement						
		2.8.2	Brief Summary of KVN Geodetic Measurement						
(Obs	erving	Proposal						
•	3.1	1 Call for Proposals (CfP)							
•	3.2	Propos	sal Submission						
•	3.3	Specia	l Condition for Selecting Proposals						
•	3.4	Observ	vation Mode						
•	3.5	Possib	le Conflict/Duplication with KaVA/EAVN Large Programs						

	3.6	Target of Opportunity (ToO) Observations	29
	3.7	Angular Resolution and Largest Detectable Angular Scale	29
	3.8	Sensitivity	30
	3.9	Calibrator Information	31
	3.10	Data Archive	32
4	Not	ses for special modes	33
	4.1	Phase-referencing and astrometry	33
		4.1.1 VERA dual-beam and KVN single-beam observations	33
		4.1.2 Tropospheric calibration with GPS and JMA data	33
		4.1.3 Delay recalculation table for precise position measurement	34
		4.1.4 Digital filter mode	34
		4.1.5 Data reduction	34
		4.1.6 Astrometric accuracy for KaVA K-band observations	34
	4.2	1-beam hybrid (K/Q/W) mode	38
	4.3	Wide-field imaging mode	38
5	Obs	servation and Data Reduction	41
	5.1	Preparation of an EAVN Observation	41
	5.2	Observation and Correlation	41
	5.3	Data Reduction	42
	5 4	Further Information	42

1 Introduction

This document describes the current observational capabilities as of 2019 September, and available observing time of the East Asian VLBI Network (EAVN). EAVN is the international collaborative VLBI array operated by Korea Astronomy and Space Science Institute (KASI), National Astronomical Observatory of Japan (NAOJ), Shanghai Astronomical Observatory (SHAO; China), and Xinjiang Astronomical Observatory (XAO; China).

EAVN invites proposals for open-use observations to be carried out from January 11 to June 10, 2020 (2020A semester). The total observing time of 500 hours is provided for EAVN open-use operation to proposers, while the available machine time of each telescope is different between each other. Please refer to Section 3 for more details.

In the 2020A semester, EAVN is operated using 11 telescopes, 7 telescopes of the KVN and VERA Array (KaVA) in Korea and Japan, Nobeyama 45-m and Takahagi 32-m telescopes in Japan, Tianma 65-m and Nanshan 26-m telescopes in China. Figure 1 shows location of EAVN telescopes which participate in open-use observations of EAVN in the 2020A semester.

This status report summarizes general information about EAVN brief summary and the performance of each telescope/array, and how to prepare and submit proposals for EAVN.



Figure 1: Location of EAVN sites, including the Korea-Japan Correlation Center at KASI, Korea, overlaid on 'the Blue Marble' image (credit of the ground image: NASA's Earth Observatory).

2 System

2.1 Array

In the 2020A semester, 11 radio telescopes (KVN 3×21 m, VERA 4×20 m, Nobeyama 45 m, Takahagi 32 m, Tianma 65 m, and Nanshan 26 m) are available for EAVN open use, as shown in Figure 1. Takahagi 32 m telescope newly participates in EAVN openuse program from the 2020A semester. Two observing frequencies, 22 (K-band) and 43 GHz (Q-band), are opened in the 2020A semester. KaVA (KVN and VERA Array) is a core array of EAVN, which consists of 7 antenna sites in VERA-Mizusawa, VERA-Iriki, VERA-Ogasawara, VERA-Ishigakijima, KVN-Yonsei, KVN-Ulsan and KVN-Tamna with 21 baselines. The maximum baseline length of KaVA is 2270 km between Mizusawa and Ishigakijima, and the minimum baseline length is 305 km between Yonsei and Ulsan. The maximum angular resolution expected from the baseline length of KaVA is about 1.2 mas for K-band and about 0.6 mas for Q-band. The maximum angular resolution is improved to be 0.55 mas at K-band for EAVN (the longest baseline is 5,100 km for VERA-Ogasawara – Nanshan baseline), while the maximum angular resolution of EAVN at Q-band is identical to that of VERA (0.63 mas for VERA-Mizusawa – VERA-Ishigakijima baseline). The geographic locations and coordinates of EAVN antennas in the coordinate system of epoch 2009.0 are summarized in Table 2.8.1. Figures 2 and 3 show examples of uv plane coverage for KaVA and EAVN, respectively.

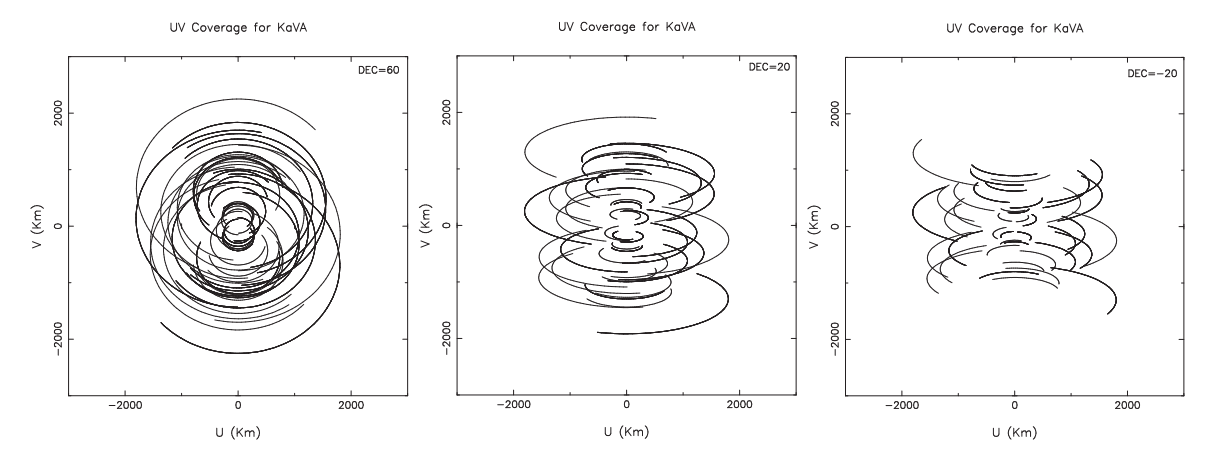


Figure 2: The uv plane coverage (± 3000 km) expected with KaVA antennas from an observation over elevation of 20°. Each panel shows the uv coverage for the declination of 60° (left), 20° (center), and -20° (right).

The coordinates and averaged velocities of VERA sites in Table 2 are predicted values at the epoch of January 1, 2018. Reference frame of these coordinates is ITRF2014. The rates of the coordinates of Mizusawa, Iriki, Ogasawara and Ishigakijima are the average value of change of the coordinates from April 16, 2016 to May 26, 2018, after the 2016 Kumamoto Earthquake ($M_j = 7.3$). The 2011 off the Pacific coast of Tohoku Earthquake ($M_j = 9.0$) brought the co-seismic large step and non-linear post-seismic movement to the coordinates of Mizusawa. Co-seismic steps of the coordinates of Mizusawa are dX = -2.0297 m, dY = -1.4111 m and dZ = -1.0758 m. The creeping continues still now, though decreased. The changes of coordinates by the post-seismic creeping are dX = -0.8574 m, dY = -0.5387 m and dZ = -0.2398 m in total from March 12, 2011 to January 1, 2015.

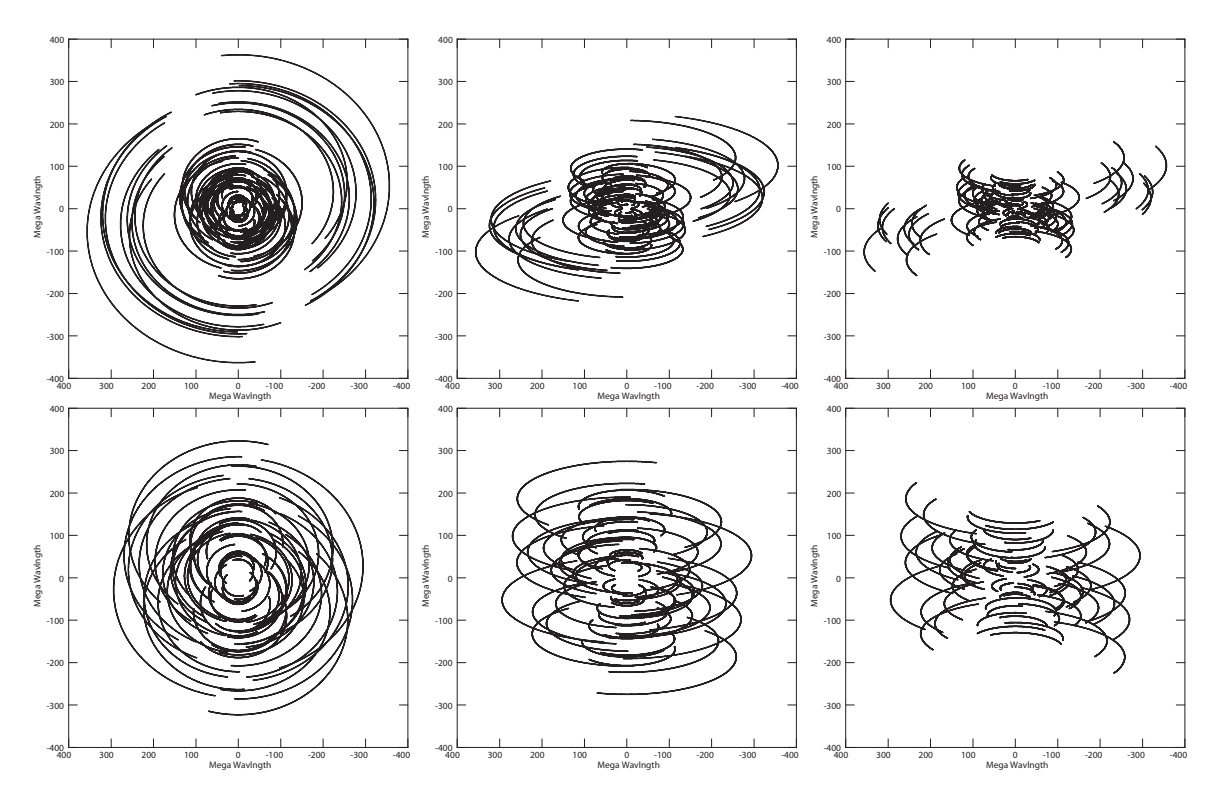


Figure 3: Examples of (u, v) coverage for an EAVN observation with full array configuration at 22 GHz (upper panels) and 43 GHz (lower panels) with the source's declination of $+60^{\circ}$ (left panels), $+20^{\circ}$ (center panels), and -20° (right panels). Total observation duration of 10 hours and the antenna's lower elevation limit of 15° are assumed for all cases.

In the case of KVN, all antenna locations are measured with GPS system. The antenna positions of KVN are regularly monitored both with GPS system and geodetic VLBI observations in collaboration with VERA. No velocity information is available for KVN stations.

2.2 Antennas

2.2.1 Brief Summary of VERA Antennas

All the telescopes of VERA have the same design, being a Cassegrain-type antenna on AZ-EL mount. Each telescope has a 20 m diameter dish with a focal length of 6 m, and with a sub-reflector of 2.6 m diameter. The dual-beam receiver systems are installed at the Cassegrain focus. Two receivers are set up on the Stewart-mount platforms, which are sustained by steerable six arms, and with such systems one can simultaneously observe two adjacent objects with a separation angle between 0.32 and 2.2 deg. The whole receiver systems are set up on the field rotator (FR), and the FR rotate to track the apparent motion of objects due to the earth rotation. Table 3 summarizes the ranges of elevation (EL), azimuth (AZ) and field rotator angle (FR) with their driving speeds and accelerations. In the case of single beam observing mode, one of two beams is placed at the antenna vertex (separation offset of 0 deg).

Table 1: Geographic locations and motions of each EAVN antenna.

	East	North	Ellipsoidal			
Site	Longitude	Latitude	Height	X	Y	${ m Z}$
	[°′″]	[° ′ ′′]	[m]	[m]	[m]	[m]
Nobeyama ^a	138 28 21.2	35 56 40.9	1350	-3871025.4987	3428107.3984	3724038.7361
$Takahagi^b$	$140\ 41\ 41.0$	$36\ 41\ 54.6$	117.0	-3961881.8250	3243372.4800	3790687.4490
$Tianma^c$	$121\ 08\ 09.4$	$30\ 55\ 19.8$	49.2	-2826708.6380	4679237.0440	3274667.5330
Nanshan	$87\ 10\ 40.4$	$43\ 28\ 15.6$	2029.4	228310.1700	4631922.7550	4367064.0740
Mizusawa ^d	141 07 57.3	39 08 00.7	116.6	-3857244.9089	3108782.9415	4003899.1770
Iriki^d	$130\ 26\ 23.6$	$31\ 44\ 52.4$	573.6	-3521719.8633	4132174.6847	3336994.1305
$Ogasawara^d$	$142\ 12\ 59.8$	$27\ 05\ 30.5$	273.1	-4491068.4253	3481545.2331	2887399.7871
Ishigakijima d	$124\ 10\ 15.6$	$24\ 24\ 43.8$	65.1	-3263995.2318	4808056.3788	2619948.6690
$Yonsei^e$	$126\ 56\ 27.4$	$37\ 33\ 54.9$	139	-3042280.9137	4045902.7164	3867374.3544
Ulsan^e	$129\ 14\ 59.3$	$35\ 32\ 44.2$	170	-3287268.7200	4023450.0790	3687379.9390
Tamna^e	$126\ 27\ 34.4$	$33\ 17\ 20.9$	452	-3171731.7246	4292678.4575	3481038.7330

^aThe position was measured in late 2016.

Table 2: Station code and average velocity of each VERA antenna.

				v		
Site	$IVS2^a$	$IVS8^b$	CDP^c	$\Delta X [m/yr]^d$	$\Delta Y [m/yr]^d$	$\Delta Z [m/yr]^d$
Mizusawa	Vm	VERAMZSW	7362	-0.0123	0.0359	-0.0166
Iriki	Vr	VERAIRIK	7364	-0.0151	0.0038	-0.0105
Ogasawara	Vo	VERAOGSW	7363	0.0378	0.0298	0.0183
Ishigakijima	$V_{\rm S}$	VERAISGK	7365	-0.0332	-0.0074	-0.0471

^aIVS 2-characters code

2.2.2 Brief Summary of KVN Antennas

The KVN antennas are also designed to be a shaped-Cassegrain-type antenna with an AZ-EL mount. The telescope has a 21 m diameter main reflector with a focal length of 6.78 m. The main reflector consists of 200 aluminum panels with a manufacturing surface accuracy of about 65 μ m. The slewing speed of the main reflector is 3 °/sec, which enables fast position-switching observations (Table 3). The sub-reflector position, tilt, and tip are remotely controlled and modeled to compensate for the gravitational deformation of the main reflector and for the sagging-down of the sub-reflector itself.

2.2.3 Nobeyama 45-m Telescope

The Nobeyama 45-m Telescope (hereafter NRO45) is one of the largest millimeter radio telescope in the world. It has a Cassegrain-Coudé optics. The paraboloidal main reflector consists of about 600 pieces of panels, each of which has a surface accuracy of about 60 microns, and the deviation of the whole antenna from an ideal paraboloid is about 90 microns. The sub-reflector has a diameter of 4 m with a convex hyperboloid surface, the position of which is computer-controlled to follow the moving focal point

^bThe position was measured in November 2015.

 $[^]c$ The epoch of the coordinate is January 1, 2014.

^dThe epoch of the coordinates is January 1, 2015.

 $[^]e$ The positions are obtained by the KaVA K-band geodesy program on January 24, 2014.

 $[^]b ext{IVS}$ 8-characters code

^cCDP (NASA Crustal Dynamics Project) code

^dThe epoch of the coordinates is January 01, 2015. Average speed was obtained from the VLBI data from January 01, 2014 to June 10, 2016.

because the main reflector deforms as the elevation angle changes. The slewing speed of the telescope is 20°/min (i.e., 0.3°/sec). The (EL, AZ) driving ranges are also summarized in Table 3. More details on the NRO45 can be found in the Nobeyama Radio Observatory official website [2].

2.2.4 Takahagi 32-m Telescope

The Takahagi 32-m Telescope (hereafter TAK32) has a shaped Cassegrain-Coude-type design with a 32-m diameter main reflector and a 2.9-m sub-reflector on Az-El mount. The telescope was constructed in 1992. Cryogenically-cooled receivers at 2 frequency bands (6 - 9 GHz) and 21 - 25 GHz are equipped. The surface accuracy of the main reflector is < 0.64 mm rms at the antenna elevation angle of 35 deg, and 1.6 mm at other antenna elevation angles. The surface accuracy of the sub-reflector is < 0.2 mm rms. The slewing rates of the main reflector is 0.07 deg/sec, as shown in Table 3. The tentative value of aperture efficiency of TAK32 is 30% at K-band (see Table 4; [9]).

2.2.5 Tianma 65-m Telescope

The Tianma 65-m Telescope (hereafter TMRT65) has a shaped Cassegrain-type design with a 65-m diameter main reflector and a 6.5-m sub-reflector on Az-El mount. The main reflector consists of 1008 aluminum panels deploying an active surface control system with 1104 actuators. The prime mirror achieves a surface accuracy of about 0.3 mm rms after compensating the gravitational deformation in real time by the active surface control system. The secondary mirror has a surface error of 0.1 mm rms. A rotatable receiver cabin with the feeds covering frequency range from S-band (2 GHz) to Q-band is mounted at the Cassegrain focus, while the L-band (1.6 GHz) feed is off focus mount separately. The slewing rates of the main reflector are 0.5°/sec in azimuth and 0.3°/sec in elevation, as shown in Table 3.

Dual-beam receivers are installed in TMRT65 at both K- and Q-bands. These two beams have a fixed separation angle of 140 arcsec at K-band and 100 arcsec at Q-band. One of the beams is placed at the antenna focus for VLBI observations. Typical sidelobe levels are 13 – 15dB at both K- and Q-bands. The measured beam sizes (HPBW) are listed in Table 4.

2.2.6 Nanshan 26-m Telescope

The Nanshan 26-m Telescope (hereafter NSRT26) has a Cassegrain-type design with a 26-m diameter main reflector and a 3-m sub-reflector on Az-El mount. The telescope was constructed in 1991 with 25-m-diameter main reflector, while refurbishment of the telescope was completed in 2015 resulting in enlargement of the main reflector of 26 m and improvement of the antenna surface accuracy. Receivers at five frequency bands, L, S/X, C, K, and Q, are equipped, while the new Q-band cooled receiver has been installed in 2018 and is under evaluation. The surface accuracy of main- and sub-reflectors are 0.18 mm rms and 0.1 mm rms, respectively. The slewing rates of the main reflector are 1.0°/sec in azimuth and 0.5°/sec in elevation, as shown in Table 3.

Table 3: Driving performance of EAVN telescopes.

		O I					
Driving axis	Driving range	Max. driving speed	Max. driving acceleration				
		Nobeyama					
AZ^a	$-60^{\circ} \sim 510^{\circ}$	$0.3^{\circ}/\text{sec}$	$0.3^{\circ}/\mathrm{sec}^2$				
EL	$12^{\circ} \sim 80^{\circ}$	$0.3^{\circ}/\mathrm{sec}$	$0.3^{\circ}/\mathrm{sec}^2$				
		Takahagi	·				
AZ^a	$11^{\circ} \sim 349^{\circ}$	$0.07^{\circ}/\mathrm{sec}$	$0.035^{\circ}/\mathrm{sec}^2$				
EL	$15^{\circ} \sim 70^{\circ}$	$0.07^{\circ}/\mathrm{sec}$	$0.035^{\circ}/\mathrm{sec^2}$				
		Tianma					
AZ^a	$-60^{\circ} \sim 425^{\circ}$	$0.5^{\circ}/\mathrm{sec}$	$0.27^{\circ}/\mathrm{sec}^2$				
EL	$8^{\circ} \sim 88^{\circ}$	$0.3^{\circ}/\mathrm{sec}$	$0.16^{\circ}/\mathrm{sec^2}$				
		Nanshan					
AZ^a	$-270^{\circ} \sim 270^{\circ}$	$1.0^{\circ}/\text{sec}$	$0.5^{\circ}/\mathrm{sec^2}$				
EL	$5^{\circ} \sim 88^{\circ}$	$0.5^{\circ}/\mathrm{sec}$	$0.5^{\circ}/\mathrm{sec}^2$				
		VERA					
AZ^a	$-90^{\circ} \sim 450^{\circ}$	$2.1^{\circ}/\text{sec}$	$2.1^{\circ}/\mathrm{sec}^2$				
EL	$5^{\circ} \sim 85^{\circ}$	$2.1^{\circ}/\mathrm{sec}$	$2.1^{\circ}/\mathrm{sec}^2$				
FR^b	$-270^{\circ} \sim 270^{\circ}$	$3.1^{\circ}/\mathrm{sec}$	$3.1^{\circ}/\mathrm{sec}^2$				
	KVN						
AZ^a	$-90^{\circ} \sim 450^{\circ}$	$3.0^{\circ}/\mathrm{sec}$	$3.0^{\circ}/\mathrm{sec}^2$				
EL	$5^{\circ} \sim 85^{\circ}$	$3.0^{\circ}/\mathrm{sec}$	$3.0^{\circ}/\mathrm{sec}^2$				
#Th th :- 00 1 th t :- 000							

^aThe north is 0° and the east is 90° .

2.2.7 Aperture Efficiency

The aperture efficiency of each VERA antenna is about 40–50% in both K- and Q-bands (see Table 4 for the 2019 and 2012 data for VERA and KVN, respectively). The latest values for VERA were measured from 2018 December to 2019 March. These measurements were based on the observations of Jupiter assuming that the brightness temperature of Jupiter is 160 K in both K- and Q-bands. Due to the bad weather condition in some of the sessions, the measured efficiencies show large scatter. However, we conclude that the aperture efficiencies are not significantly changed compared with previous measurements. The elevation dependence of aperture efficiency for VERA antenna was also measured from the observation toward maser sources. Figure 4 shows the relations between the elevation and the aperture efficiency measured for VERA Iriki

Table 4: Aperture efficiency and beam size of EAVN telescopes.

	K-band (22 GHz)		Q-ban	d (43 GHz)
	$\overline{\eta_{\mathrm{A}}}$	HPBW	$\overline{\eta_{ m A}}$	HPBW
Telescope name	(%)	(arcsec)	(%)	(arcsec)
Nobeyama	61	72	53	39
Takahagi	30	100	_	_
Tianma	50	44	50	22
Nanshan	60	115	_	_
Mizusawa	48	139	50	68
Iriki	45	136	41	72
Ogasawara	41	134	43	72
Ishigakijima	47	141	47	73
Yonsei	55	127	63	63
Ulsan	63	124	61	63
Tamna	60	126	63	63

^bField rotator. FR is 0° when Beam-1 is at the sky side and Beam-2 is at the ground side, and CW is positive when a telescope is seen from a target source.

station. The gain curves are measured by observing the total power spectra of intense maser sources. The aperture efficiency in low elevation of ≤ 20 deg decreases slightly, but this decrease is less than about 10%. Concerning this elevation dependence, the observing data FITS file include a gain curve table (GC table), which is AIPS readable, in order to calibrate the dependence when the data reduction.

The aperture efficiency and beam size for each KVN antenna are also listed in Table 4. Aperture efficiency of KVN varies with elevation as shown in Figure 4. The main reflector panels of KVN antennas were installed to give the maximum gain at the elevation angle of 48°. The sagging of sub-reflector and the deformation of main reflector by gravity with elevation results in degradation of antenna aperture efficiency with elevation. In order to compensate this effect, KVN antennas use a hexapod to adjust sub-reflector position. Figure 4 shows the elevation dependence of antenna aperture efficiency of the KVN 21 m radio telescopes measured by observing Venus or Jupiter. By fitting a second order polynomial to the data and normalizing the fitted function with its maximum, we derived a normalized gain curve which has the following form:

$$G_{\text{norm}} = A_0 E L^2 + A_1 E L + A_2,$$
 (1)

where EL is the elevation in degree.

Aperture efficiency and beam size for non-KaVA telescopes are also summarized in Table 4. The values for NRO45 are based on the latest measurements in autumn 2017, where the Jupiter or the Mars was used as a reference source. The elevation dependence of the aperture efficiency is approximately constant over a range of El $\sim 25^{\circ} - 50^{\circ}$ at both K- and Q-bands.

The aperture efficiency of TMRT65 is above 50% at both K- and Q-bands with the active surface control system. The main reflector panels were assembled to give the maximum surface accuracy at the elevation angle of 52° . The aperture efficiency goes down to less than 10% at low ($<10^{\circ}$) and high ($>80^{\circ}$) elevation angles, mainly due to the gravitational deformation. The active surface control system is used for compensating the gravitational effect at different elevation angles, making the gain curves as a constant over the elevation. Figure 5 shows the elevation dependence of the aperture efficiency at Q-band with or without the active surface control. The active surface control system is set 'ON' by default at K- and Q-band observations.

The aperture efficiency of TAK32 and NSRT26 is 30% and 60% at K-band, respectively.

2.2.8 Beam Pattern and Size

Figure 6 shows the beam patterns for VERA at K-band. The side-lobe level is less than about $-15 \, \mathrm{dB}$, except for the relatively high side-lobe level of about $-10 \, \mathrm{dB}$ for the separation angle of 2.0 deg at Ogasawara station. The side-lobe of the beam patterns has an asymmetric shape, but the main beam has a symmetric Gaussian shape without dependence on separation angle. The measured beam sizes (HPBW) in K- and Q-bands based on the data of the pointing calibration are also summarized in Table 4. The main beam sizes show no dependence on the dual-beam separation angle.

The optics of KVN antenna is a shaped Cassegrain type of which the main reflector and subreflector are shaped to have a uniform illumination pattern on an aperture plane. Because of the uniform illumination, KVN antennas can get higher aperture

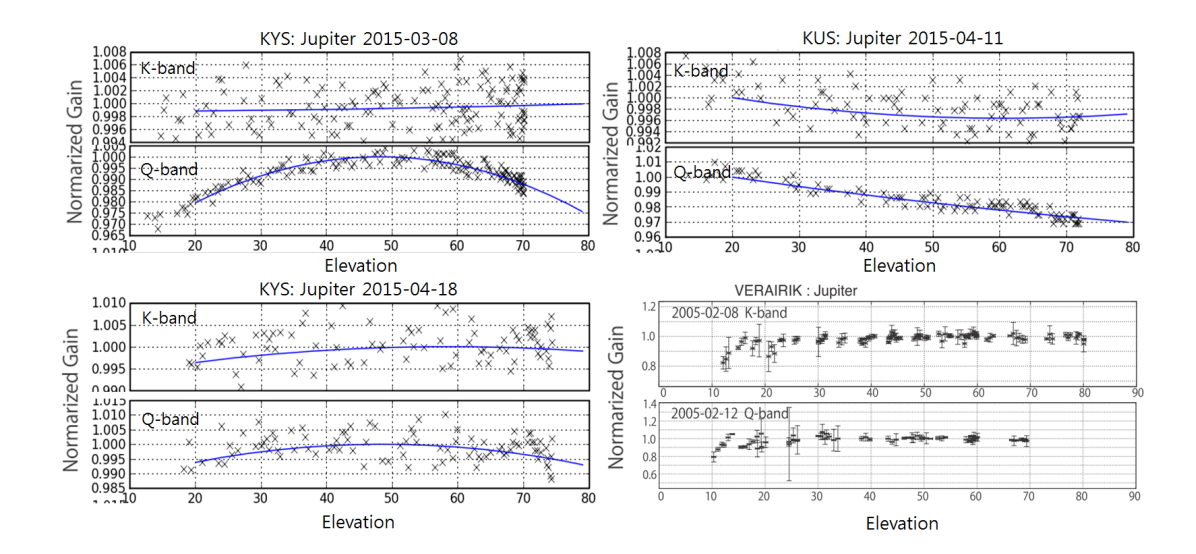


Figure 4: The elevation dependence of the aperture efficiency for KVN three antennas and VERA Iriki antenna. For KVN antennas, the maximum gain is given at the elevation angle of 48°. The efficiency in K-band (on Feb 8, 2005) and the Q-band (on Feb 12, 2005) for VERA Iriki antenna is shown in *bottom right*. The efficiency is relative value to the measurement at $EL = 50^{\circ}$.

efficiency than value of typical Cassegrain type antenna. However, higher side-lobe level is inevitable. OTF images of Jupiter at K- and Q-bands are shown in Figure 6. The map size is $12'\times10'$ and the first side-lobe pattern is clearly visible. Typical side-lobe levels of KVN antennas are 13-14dB.

2.3 Receivers

2.3.1 Brief Summary of VERA Receiving System

Each VERA antenna has the receivers for 4 bands, which are S (2 GHz), C (6.7 GHz), X (8 GHz), K (22 GHz), and Q (43 GHz) bands. For the open use, K-band and Q-band are open for observation. The low-noise HEMT amplifiers in the K- and Q-bands are enclosed in the cryogenic dewar, which is cooled down to 20 K, to reduce the thermal noise. The range of observable frequency and the typical receiver noise temperature $(T_{\rm RX})$ at each band are summarized in Table 5 and Figure 7.

After the radio frequency (RF) signals from astronomical objects are amplified by the receivers, the RF signals are mixed with standard frequency signal generated in the first local oscillator to down-convert the RF to an intermediate frequency (IF) of $4.7~\mathrm{GHz}-7~\mathrm{GHz}$. The first local frequencies are fixed at $16.8~\mathrm{GHz}$ in K-band and at $37.5~\mathrm{GHz}$ in Q-band. The IF signals are then mixed down again to the base band frequency of $0-512~\mathrm{MHz}$. The frequency of second local oscillator is tunable with a possible frequency range between 4 GHz and 7 GHz. The correction of the Doppler effect due to the earth rotation is carried out in the correlation process after the observation. Therefore, basically the second local oscillator frequency is kept to be constant during the observation. Figure 8 shows a flow diagram of these signals for VERA.

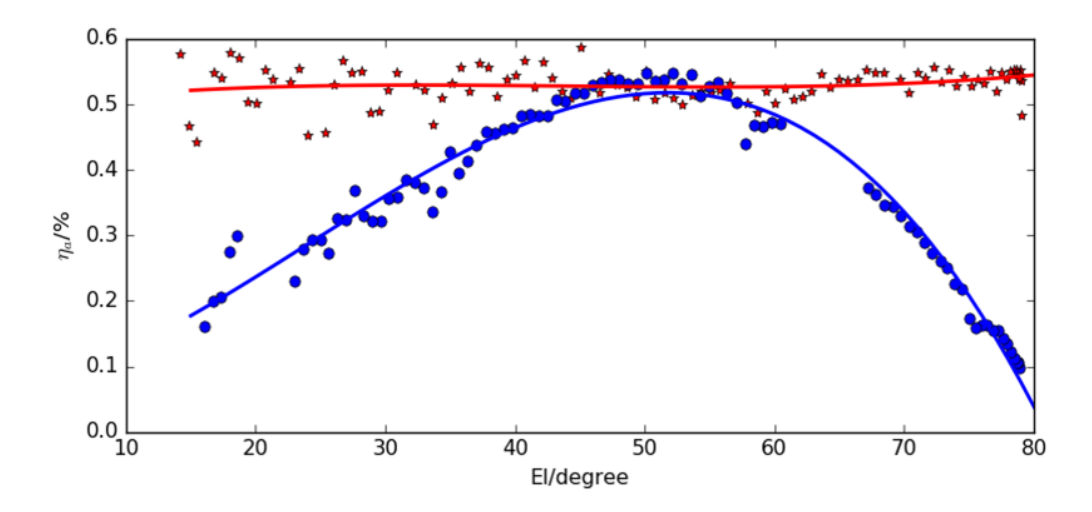


Figure 5: Elevation dependence of the aperture efficiency (η_{eff}) for TMRT65 at Q-band. The red and blue colors represent η_{eff} with or without the active surface control, respectively.

2.3.2 Brief Summary of KVN Receiving System

The KVN quasi-optics are uniquely designed to observe 22, 43, 86 and 129 GHz band simultaneously [4], [5]. Figure 9 shows the layout of quasi-optics and receivers viewing from sub-reflector side. The quasi-optics system splits one signal from sub-reflector into four using three dichroic low-pass filters marked as LPF1, LPF2 and LPF3 in the Figure 9. The split signals into four different frequency bands are guided to corresponding receivers.

Figure 10 shows a signal flows in KVN system. The 22, 43 and 86 GHz band receivers are cooled HEMT receivers and the 129 GHz band receiver is a SIS mixer receiver. All receivers can receive dual-circular-polarization signals. Among eight signals (four dual-polarization signals), four signals selected by the IF selector are down-converted to the input frequency band of the sampler. The instantaneous bandwidth of the 1st IF of each receiver is limited to 2 GHz by the band-pass filter. The 1st IF signal is down-converted by BBCs to the sampler input frequency (512 – 1024 MHz) band.

Typical noise temperatures of K- and Q-bands are presented in Table 5. Since the calibration chopper is located before the quasi-optics as shown in Figure 9, the loss of quasi-optics contributes to receiver noise temperature instead of degrading antenna aperture efficiency. Therefore, the noise temperature in the table includes the contribution due to the quasi-optics losses.

The receiver noise temperatures of three stations are similar to each other except that the noise temperature of the Ulsan 43 GHz because of the different type of thermal isolator, which is used to reduce heat flow from the feed horn in room temperature stage to cryogenic cooled stage more effectively.

2.3.3 Brief Summary of NRO45 Receiving System

The NRO45 covers an observing frequency range of 20 - 116 GHz with multiple receivers. The VLBI backend system of the NRO45 is currently equipped at K-band

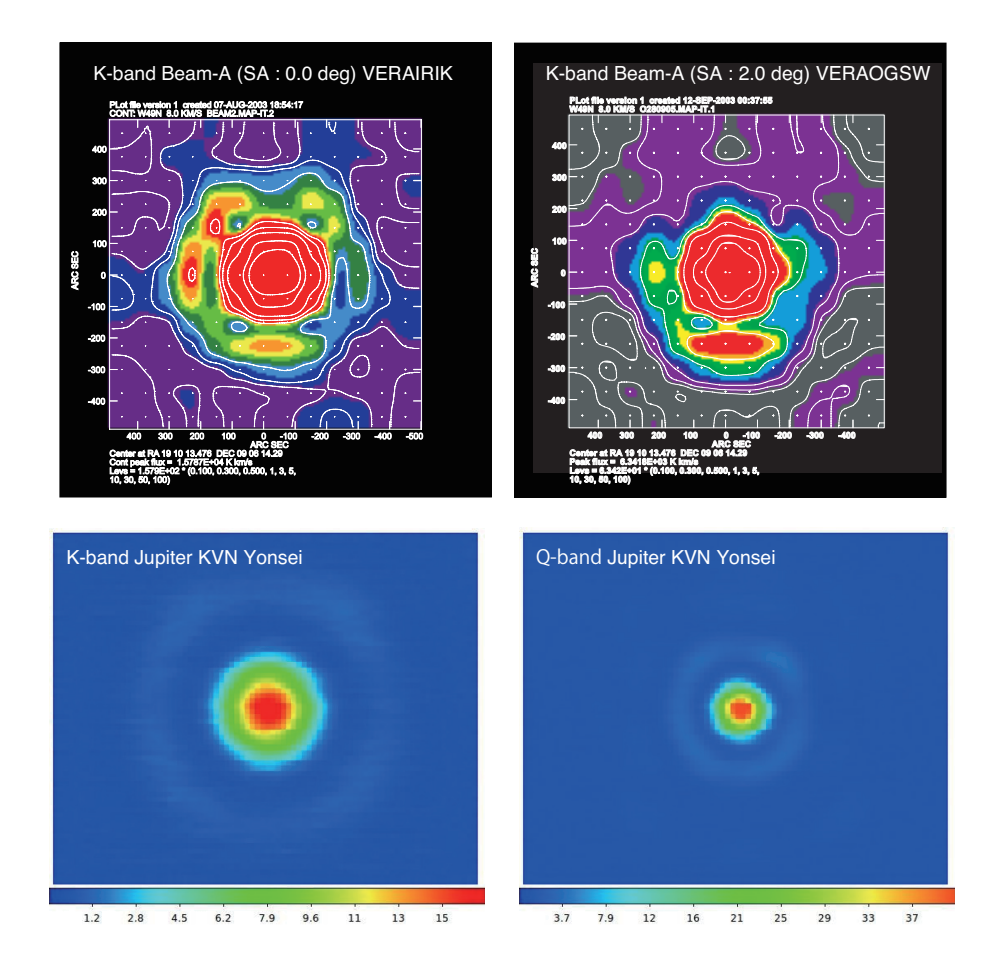


Figure 6: The beam patterns in the K-band for VERA (A-beam) Iriki with the separation angle of 0° (*Upper left*) and Ogasawara with the separation angle of 2.0° (*Upper right*), and in K/Q-band for KVN Yonsei. The patterns of VERA antennas were derived from the mapping observation of strong H₂O maser toward W49N, which can be assumed as a point source, with grid spacing of 75". In the case of KVN antennas, the patterns were derived from the OTF images of Venus at K/Q-band.

and Q-band. Figure 11 illustrates a flow diagram of the VLBI receiving system in the NRO45. The observable RF range and typical receiver noise temperature for the receivers at K- and Q-bands are also summarized in Table 5. The received RF signals are down-converted into an IF range of 5-7 GHz, and the IF signals are then mixed down to the base band of 512-1024 MHz, which is the input to the A/D sampler.

Currently, one of the receivers can be selected by switching the mirrors in the optics in a few minutes manually. In the near future, K- and Q-band observations can be conducted simultaneously by inserting a perforated high-pass dichroic plate. When using the dichroic plate, the gain of the Q-band signals may be reduced by 0.3dB (in 2018 June), causing the rise of the system noise temperature by about 30 K.

2.3.4 Brief Summary of TAK32 Receiving System

Figure 12 shows a flow diagram of the VLBI receiving system in TAK32. TAK32 covers an observing frequency range of 6-9 GHz and 21-25 GHz with two criogenically-cooled receivers, while TAK32 joins in EAVN observations at only K-band in the 2020A

Table 5: Frequency range and T_{RX} of receivers at each EAVN telescope.

Band	Frequency Range	$T_{\mathrm{RX}}{}^{a}$	Polarization				
Dana	[GHz]	[K]	1 0101111111111				
		Nobeyama					
K	21.5 - 23.8	~ 85	LCP/RCP				
Q	42.5 - 44.5	~ 111	LCP				
		Takahagi					
K	21.0 - 25.0	~ 30	LCP/RCP				
		Tianma					
K	18.0 - 26.5	16 - 35	LCP/RCP				
Q	39 - 47	35 - 50	LCP/RCP				
	Nanshan						
K	22.0 - 24.2	~ 15	LCP/RCP				
Q		(under evaluation)					
		VERA					
K	21.5 - 23.8	30 - 50	LCP				
Q	42.5 - 44.5	70 - 90	LCP				
	KVN						
K	18 - 26	20 - 40	LCP/RCP				
Q	42.11 - 44.11	70 - 80	LCP/RCP				
		(40 - 50 for Ulsan)					
a Daggiyan najag tampanatura							

^aReceiver noise temperature

semester.

The flow diagram of TAK32 is shown in Figure 12. The K-band receiver is cooled with dual circular polarization. The observable frequency range and the typical receiver noise temperature are shown in Table 5. The total system noise temperatures at K-band is typically 40 K at winter with good weather, > 100 K at winter with bad weather, 150 K at summer with good weather, and > 500 K at summer with bad weather.

For K-band, received RF signals are down-converted into an IF range of $8.0-8.8~\mathrm{GHz}$, and the IF signals are then mixed down to the base band of $512-1024~\mathrm{MHz}$, which is the input to the A/D sampler ADS-3000+. The data with the rate of $1024~\mathrm{MHz} \times 2~\mathrm{bit}$ are recorded by OCTADISK, and then the digital base-band converter is used to convert the 2 Gbps data into 1 Gbps.

2.3.5 Brief Summary of TMRT65 Receiving System

Figure 13 shows a flow diagram of the VLBI receiving system in TMRT65. TMRT65 has the receivers for 8 frequency bands, L (1.4 GHz), S/X (2.3/8.4 GHz), C (6.7 GHz), X/Ka (8.4/31.0 GHz), Ku (15 GHz), K (22 GHz), and Q (43 GHz). The K- and Q-band receivers are cooled HEMT receivers with dual circular polarizers. The observable frequency range and the typical receiver noise temperature are shown in Table 5. The total system noise temperatures at K- and Q-bands are typically 70 and 110 K, respectively. The RF signal is firstly down-converted to IF range of 4-12 GHz and it is transferred by optical fibers to the observing room, where the signal is further down-converted to 0-1024 MHz (actually in 10-512 MHz and 512-1024 MHz) at the input of BBCs.

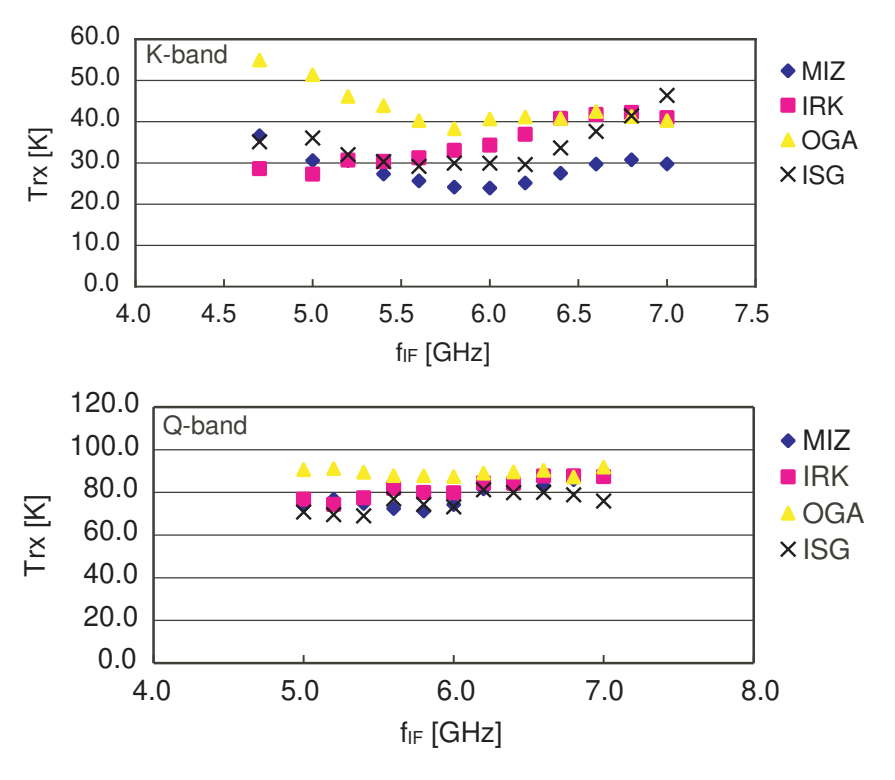


Figure 7: Receiver noise temperature for each VERA antenna. Top and bottom panels show measurements in the K- and Q-bands, respectively. Horizontal axis indicate an IF (intermediate frequency) at which $T_{\rm RX}$ is measured. To convert it to RF (radio frequency), add 16.8 GHz in K-band and 37.5 GHz in Q-band to the IF frequency.

2.3.6 Brief Summary of NSRT26 Receiving System

Figure 14 shows a flow diagram of the VLBI receiving system in NSRT26. NSRT26 has the receivers for 5 frequency bands, L (1.4 GHz), S/X (2.3/8.4 GHz), C (5 GHz), K (22 GHz), and Q (43 GHz), while NSRT26 joins in EAVN observations at only K-band in the 2020A semester. The K-band receiver is cooled HEMT receivers with dual circular polarizers. The observable frequency range and the typical receiver noise temperature are shown in Table 5. The total system noise temperatures at K-band is typically 42 K. The RF signal is down-converted with three stages, and analog-digital conversion and digital filtering of the IF signal is conducted using either the Digital Baseband Converter (DBBC) system or the Chinese VLBI Data Acquisition System (CDAS).

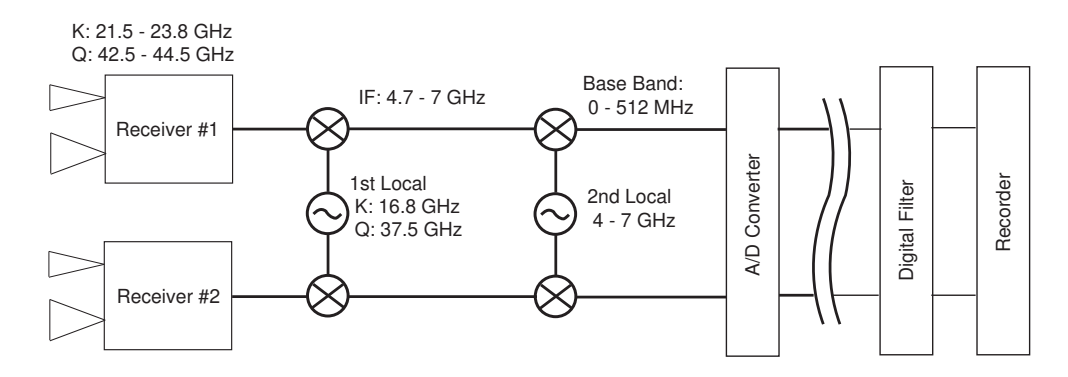


Figure 8: Flow diagram of signals from receiver to recorder for VERA.

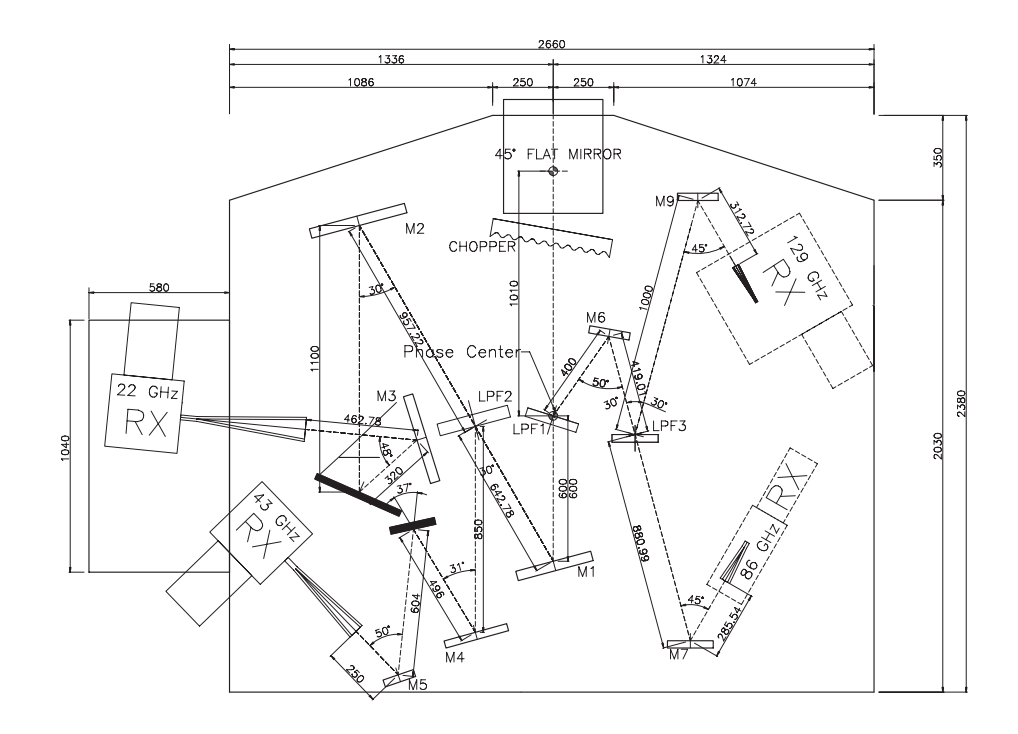


Figure 9: KVN multi-frequency receiving system [4], [5].

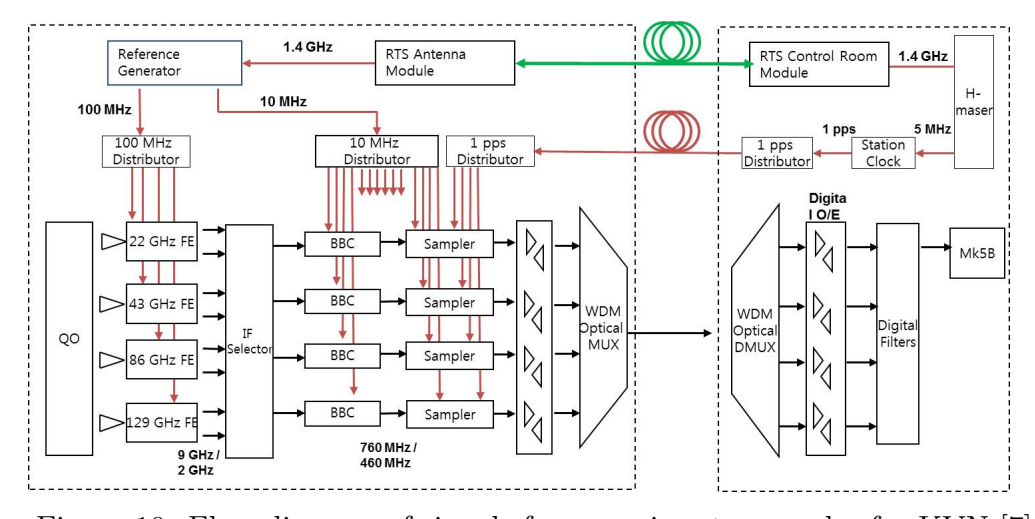


Figure 10: Flow diagram of signals from receiver to recorder for KVN [7].

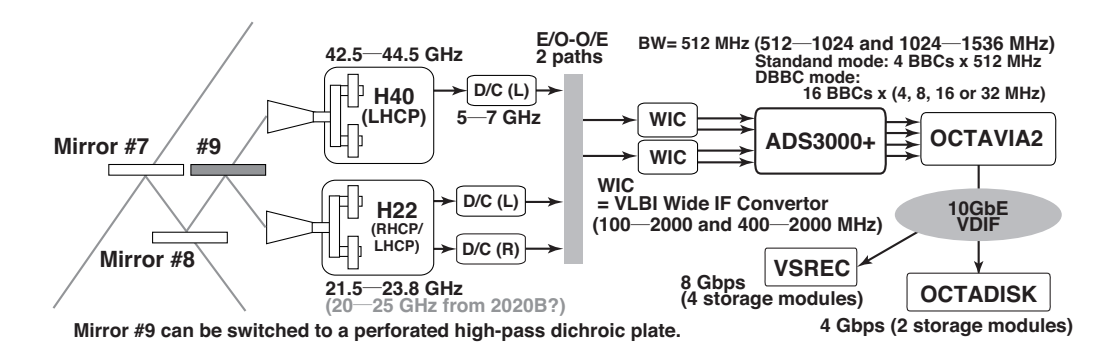


Figure 11: Flow diagram of signals from receiver to recorder for NRO45.

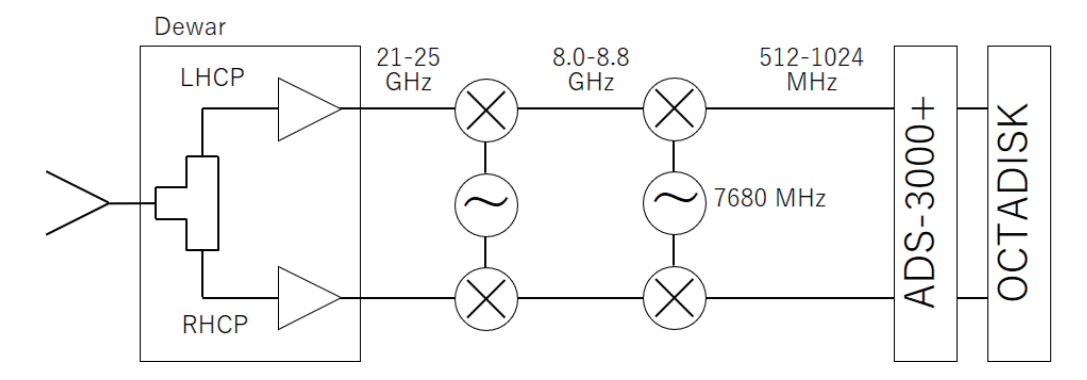


Figure 12: Flow diagram of signals from receiver to recorder for TAK32.

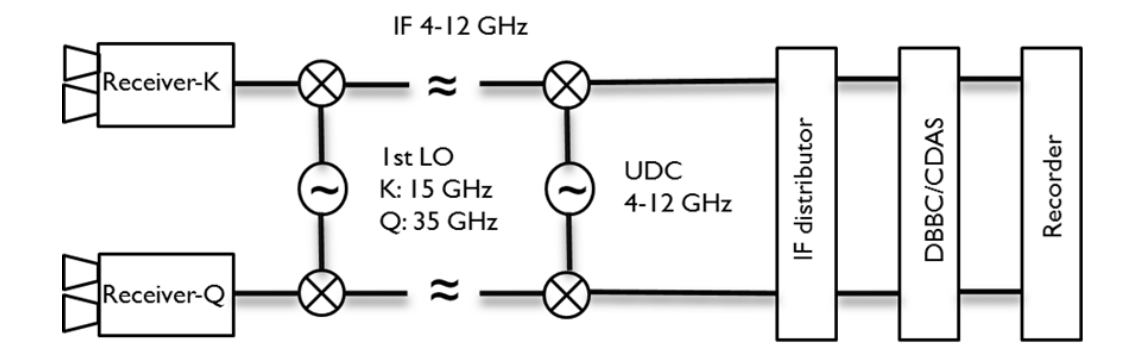


Figure 13: Flow diagram of signals from receiver to recorder for TMRT65.

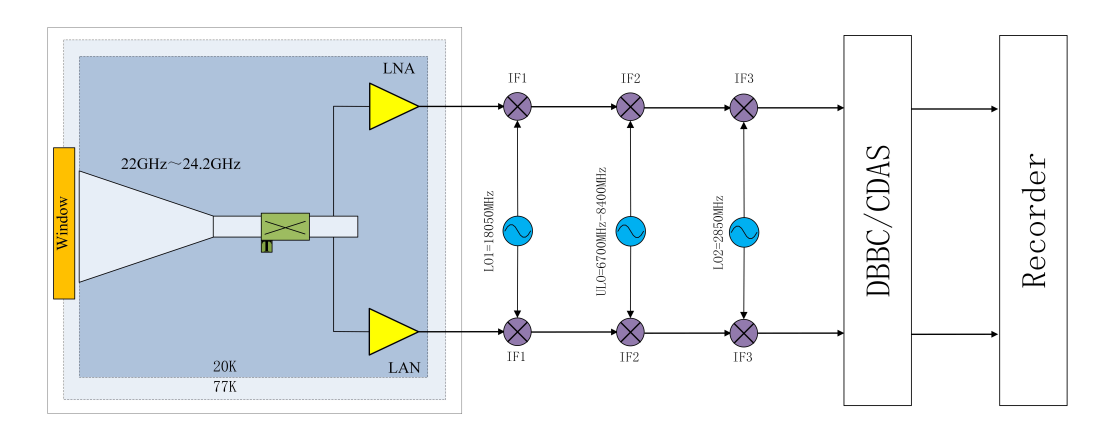


Figure 14: Flow diagram of signals from receiver to recorder for NSRT26.

2.4 Digital Signal Processing

In VERA system, A/D (analog-digital) samplers convert the analog base band outputs of 0-512 MHz \times 2 beams to digital form. The A/D converters carry out the digitization of 2-bit sampling with the bandwidth of 512 MHz and the data rate is 2048 Mbps for each beam.

In KVN system, A/D samplers digitize signals into 2-bit data streams with four quantization levels. The base band output is 512 - 1024 MHz. The sampling rate is 1024 Mega sample per second (Msps) with 2-bit sampling, resulting in the data rate of 2 Gbps at the frequency bandwidth of 512 MHz. Four streams of 512 MHz band width (2 Gbps data rate) can be obtained in the KVN multi-frequency receiving system simultaneously, which means that the total rate is 8 Gbps.

In NRO45 system, the baseband signal output is 512 - 1024 MHz and the A/D samplers perform 2-bit digitization with four quantization levels. A maximum recording rate of 2048 Mbps is possible with a total bandwidth of 512 MHz.

Since the total data recording rate is limited to 1024 Mbps (see the next section), only part of the sampled data can be recorded onto hard disks. The data rate reduction is done by digital filter system, with which one can flexibly choose number and width of recording frequency bands.

Observers can select modes of the digital filter listed in the Table 6. In VERA7SIOS mode in the Table 6, two transitions (v=1 & 2) of SiO maser in the Q band can be simultaneously recorded. Digital filter modes of VERA1, VERA7, and VERA7MM are available for dual-beam astrometry with VERA (see section 4.1).

2.5 Recorders

The EAVN observations are basically limited to record with 1024 Mbps data rate. To response 1 Gbps recording, VERA, NRO45, and TAK32 have OCTADISK. KVN, TMRT65, and NSRT26 use the Mark5B recording systems. OCTADISK and Mark5B are hard disk recording systems developed at NAOJ and Haystack observatory, respectively. The total bandwidth is 256 MHz.

2.6 Correlators

The correlation process is carried out by a VLBI correlator located at KJCC (Korea-Japan Correlation Center) at Daejeon, which has been developed as the KJJVC (Korea-Japan Joint VLBI Correlator) located at KJCC (Korea-Japan Correlation Center) project. Hereafter it is tentatively called "Daejeon correlator". Specification of The Daejeon correlator is summarized in Table 8. The Daejeon correlator can process the data stream of up to 8192 Mbps from maximum 16 antenna stations at once. Currently the raw observed data of KVN, TMRT65, and NSRT26 stations are recorded and playbacked with Mark5B, and those of VERA, NRO45, and TAK32 are recorded and playbacked with OCTADISK at the data rate of 1024 Mbps. For KaVA, data formats available in the next observing season are 16 IFs × 16 MHz ("C5 mode" in The Daejeon correlator terminology), 8 IFs × 32 MHz (C4 mode), and 2 IFs × 128 MHz (C2 mode). For EAVN (including non-KaVA telescopes), available data formats are 16 IFs × 16 MHz (C5 mode) at K-band, and 8 IFs × 32 MHz (C4 mode) at both K-

Table 6: Digital filter mode for EAVN.

Mode	Rate	Num.	$\mathrm{BW}/\mathrm{CH}^b$		Freq. range ^{d}	Side	
Name	(Mbps)	CH^a	(MHz)	CH^c	(MHz)	Band^e	Note^f
GEO1K*	1024	16	16	1	0 - 16	U	
				2	32 - 48	U	
				3	64 - 80	U	
				4	96 - 112	U	
				5	128 - 144	U	
				6	160 - 176	U	
				7	192 - 208	U	
				8	224 - 240	U	
				9	256 - 272	U	Target line (e.g. H_2O)
				10	288 - 304	U	
				11	320 - 336	U	
				12	352 - 368	U	
				13	384 - 400	U	
				14	416 - 432	U	
				15	448 - 464	U	
				16	480 - 496	U	
GEO1S*	1024	16	16	1	112 - 128	L	
				2	128 - 144	U	
				3	144 - 160	${ m L}$	
				4	160 - 176	U	
				5	176 - 192	${ m L}$	
				6	192 - 208	U	
				7	208 - 224	${ m L}$	
				8	224 - 240	U	
				9	240 - 256	${ m L}$	
				10	256 - 272	U	Target line (e.g. H_2O)
				11	272 - 288	${ m L}$	
				12	288 - 304	U	
				13	304 - 320	${ m L}$	
				14	320 - 336	U	
				15	336 - 352	${ m L}$	
				16	352 - 368	U	
VERA7SIOS*	1024	16	16	1	32 - 48	U	
				2	64 - 80	U	
				3	80 - 96	L	SiO $(J=1-0, v=2)$
				4	96 - 112	U	
				5	128 - 144	U	
				6	160 - 176	U	
				7	192 - 208	U	
				8	224 - 240	U	
				9	256 - 272	U	
				10	288 - 304	U	
				11	384 - 400	U	SiO $(J=1-0, v=1)$
				12	320 - 336	U	, , ,
				13	352 - 368	U	
				14	416 - 432	Ü	
				15	448 - 464	Ü	
				16	480 - 496	Ü	
* All channels a	ro for A B	Ponm (VI	FRA) and I		ERA/KVN). Mo		os aro tontativo

^{*}All channels are for A-Beam (VERA) and LCP (VERA/KVN). Mode names are tentative. $^a\mathrm{Total}$ number of channels

 $[^]b\mathrm{Bandwidth}$ per channel in MHz

^cChannel number

 $[^]d\mathrm{Filtered}$ frequency range in the base band (MHz) $^e\mathrm{Side}$ Band (LSB/USB)

fExample of spectral line setting

Table 7: Digital filter mode for EAVN — continued.

Mode	Rate	Num.	$\overline{\mathrm{BW/CH}^b}$		$\frac{\text{EAVIV} - \text{Con}}{\text{Freq. range}^d}$	Side	
Name	(Mbps)	CH^a	(MHz)	CH^c	(MHz)	Band^e	Note^f
VERA4S*	1024	8	32	1	128 - 160	U	11000
, 13101112	10-1	Ü	5-	$\overset{1}{2}$	160 - 192	Ĺ	
				3	192 - 224	U	
				4	224 - 256	${ m L}$	
				5	256 - 288	U	
				6	288 - 320	${ m L}$	
				7	320 - 352	U	
				8	352 - 384	${ m L}$	
VERA1S*	1024	2	128	1	128 - 256	L	
				2	256 - 384	U	
VERA1**	1024	2	128	1	256 - 384	U	A-Beam
				2	256 - 384	U	B-Beam
VERA7**	1024	16	16	1	256 - 272	U	A-Beam for target line
				2	128 - 144	U	B-Beam (CH 2-16)
				3	144 - 160	${ m L}$	
				4	160 - 176	U	
				5	176 - 192	${ m L}$	
				6	192 - 208	U	
				7	208 - 224	${ m L}$	
				8	224 - 240	U	
				9	240 - 256	${ m L}$	
				10	256 - 272	U	
				11	272 - 288	L	
				12	288 - 304	U	
				13	304 - 320	L	
				14	320 - 336	U	
				15	336 - 352	L	
77DD 4 = 3 (5 (5 ***	1004	1.0	1.0	16	352 - 368	U	A.D. C. + 11
VERA7MM**	1024	16	16	1	256 - 272	U	A-Beam for target line
				2	32 - 48	U	B-Beam (CH 2-16)
				3	64 - 80	U	
				4	96 - 112	U	
				5 6	128 - 144	U	
				6 7	160 - 176	U	
					192 - 208	U	
				8 9	224 - 240 256 272	U U	
					256 - 272 288 - 304	U	
				10 11	200 - 304 320 - 336	U	
				$\frac{11}{12}$	352 - 368	U	
				13	384 - 400	U	
					416 - 432	U	
				$\begin{array}{c} 14 \\ 15 \end{array}$	448 - 464	U	
				16	480 - 496	U	
*All channels are	for A Ros	m (VEI	(A) and I CI				

^{*}All channels are for A-Beam (VERA) and LCP (VERA/KVN).
** New mode for the phase referencing (see section 4.1).

^aTotal number of channels

 $[^]b{\rm Bandwidth}$ per channel in MHz

 $[^]c$ Channel number

 $[^]d\mathrm{Filtered}$ frequency range in the base band (MHz)

^eSide Band (LSB/USB)

and Q-bands. Note that the C2 mode is available at only KaVA 7 telescopes. Minimum integration times (time resolution) are 0.2048, 0.8192, and 1.6384 seconds for C2, C4, and C5 modes, respectively, and the number of frequency channels within each IF is 8192 for both modes (i.e. maximum frequency resolution is about 1.95 kHz). By default, the number of frequency channels is reduced to 128 (for continuum) or 512 (for line) via channel integration after correlation. One may put a special request of number of frequency channels to take better frequency resolution. The number of frequency channels can be selected among 512, 1024, 2048, 4096 or 8192. Final correlated data is served as FITS-IDI file.

2.6.1 Note for the C2 mode

To obtain the accurate amplitude values across the all IF channels, however, it is better to reduce the number of baseband (or IFs in data handling with AIPS) yielded by the digital filter unit (DFU) so that the amplitude losses at the edge of each baseband are avoided. This reduction is especially helpful to observe continuum sources, such as active galactic nuclei (AGN). For this purpose, C2 mode, which has 2 IFs \times 128 MHz, is opened for EAVN although the mode can be employed for an observation with only KaVA 7 telescopes.

When using the C2 mode, note the following two matters: (i) There is a moderate amplitude slope in an IF channel mainly at VERA stations, which must be corrected by all the gain calibration procedures in AIPS (AIPS tasks ACCOR, BPASS, and APCAL): (ii) KaVA's observation data is conventionally correlated by the Daejeon Hardware Correlator. In this case, the scaling factor of 1.3 should be applied to the data to recover the quantization loss ¹ [6].

Table 8: Specification of The Daejeon correlator^a.

rable of specified	Tuble 6. Specification of The Bacjoon correlator.					
Max. number of antennas	16					
correlation mode	$C2^b$ (128 MHz Bandwidth, 2 stream)					
	C4(32 MHz Bandwidth, 8 stream)					
	C5(16 MHz Bandwidth, 16 stream)					
Max. number of corr./input	120 cross + 16 auto					
Sub-array	$2 \operatorname{case}(12+4, 8+8)$					
Bandwidth	512 MHz					
Max. data rate/antenna	2048 Mbps VSI-H(32 parallels, 64MHz clock)					
Max. delay compensation	$\pm~36,000~\mathrm{km}$					
Max. fringe tracking	$1.075~\mathrm{kHz}$					
FFT work length	16+16 bits fixed point for real, imaginary					
Integration time	$25.6~\mathrm{msec} \sim 10.24~\mathrm{sec}$					
Data output channels	8192 channels					
Data output rate	Max. 1.4GB/sec at 25.6msec integration time					

^aFor more details, see the following website:

http://kvn.kasi.re.kr/status_report/correlator_status.html

^bThis mode is available for only KaVA.

¹This scaling factor is conventionally applied to the data using the AIPS task APCAL, however this is not applicable if the data is loaded to AIPS using the AIPS task FITLD with DIGICOR = 3.

2.7 Calibration

Here we briefly summarize the calibration procedure of the EAVN data. Basically, most of the post-processing calibrations are done by using the AIPS (Astronomical Image Processing System) software package developed by NRAO (National Radio Astronomical Observatory).

2.7.1 Delay and Bandpass Calibration

The time synchronization for each antenna is kept within 0.1 μ sec using GPS and high stability frequency standard provided by the hydrogen maser. To correct for clock parameter offsets with better accuracy, bright continuum sources with accurately-known positions should be observed at usually every 60-80 minutes during observations. A recommended scan length for calibrators is 5-10 minutes. This can be done by the AIPS task FRING. The calibration of frequency characteristic (bandpass calibration) can be also done based on the observation of bright continuum source. This can be done by the AIPS task BPASS.

2.7.2 Gain Calibration

VERA, KVN, NRO45, and TAK32 antennas have the chopper wheel of the hot load (black body at the room temperature), and the system noise temperature can be obtained by measuring the ratio of the sky power to the hot load power (so-called R-Sky method). Thus, the measured system noise temperature is a sum of the receiver noise temperature, spillover temperature, and contribution of the atmosphere (i.e. so-called $T_{\rm sys}^*$ corrected for atmospheric opacity). The hot load measurement can be made before/after any scan at all telescopes except TAK32. TAK32 measures the system noise temperature at the timing of when the telescope operator decides the measurement before or after any scan. Also, the sky power is continuously monitored during scans, so that one can trace the variation of the system noise temperature. The system noise temperature value can be converted to SEFD (System Equivalent Flux Density) by dividing by the antenna gain in K/Jy, which is derived from the aperture efficiency and diameter of each antenna.

For the correlated data from KJCC, $T_{\rm sys}^*$ data (TY table) and antenna gain information (GC table) are provided with the ANTAB-readable format. KJCC makes complete version of ANTAB-readable file and provide it to PI. User support team supports PIs as appropriate. The TY and GC tables can be loaded by the AIPS task ANTAB, and these tables are converted to the SN table by the AIPS task APCAL.

On the other hand, $T_{\rm sys}$ measurement provided by TMRT65 and NSRT26 contains atmospheric opacity effects, thus the opacity correction should be applied to those data in the course of data reduction.

Alternatively, one can calibrate the visibility amplitude by the template spectrum method, in which auto-correlation spectra of a maser source is used as the flux calibrator. This calibration procedure is made by the AIPS task ACFIT (see AIPS HELP for ACFIT and Cho et al. (2017) [3] for more details). For an EAVN observation including TMRT65, NRO45, TAK32, and NSRT26, we strongly recommend users to observe a maser source or a compact continuum gain calibrator for every ≤ 1 hr. This offers an additional cross-check of the amplitude calibration for TMRT65/NRO45. Along with

this, these two telescopes will do regular antenna pointing scans for every $\leq 1-2$ hr.

As for TMRT65, moreover, frequent pointing check is necessary for observations at both K- and Q-bands. The pointing check is done semi-automatically with a continuum back-end system and the quality of pointing check is judged by on-site operators. We strongly recommend to keep at least 3 minutes for the pointing check itself with additional slewing time between target and pointing sources. For example, it is preferable to secure 5-min gap in total for the pointing check toward a pointing source with the angular separation of $\sim 15^{\circ}$ from the target.

Further correction is made for VLBI observations taken with 2-bit (4-level) sampling, for the systematic effects of non-optimal setting of the quantizer voltage thresholds. This is done by the AIPS task ACCOR. Another correction should be applied to recover the amplitude loss, which are attributed to the combination of two steps of 2-bit quantization in the digital filtering at the backend system and characteristics of Daejeon correlator. This is done by multiplying the scaling factor of 1.3 (the best current estimation) [6] in the AIPS task APCAL (adverbs APARM(1) = 1.3, OPCODE = ", and DOFIT = 1) or SNCOR (adverbs OPCODE = "MULA", and SNCORPRM(1) = 1.3). Note that this correction should be applied to all EAVN telescopes. The amplitude calibrations with EAVN are accurate to 15% or better at both K- and Q-bands.

2.8 Geodetic Measurement

2.8.1 Brief Summary of VERA Geodetic Measurement

Geodetic observations are performed as part of the VERA project observations to derive accurate antenna coordinates. The geodetic VLBI observations for VERA are carried out in the S/X-bands and also in the K-band. The S/X-bands are used in the domestic experiments with the Geographical Survey Institute of Japan and the international experiments called IVS-T2. On the other hand, the K-band is used in the VERA internal experiments. We obtain higher accuracy results in the K-band compared with the S/X-bands. The most up-to-date geodetic parameters are derived through geodetic analyses.

Non-linear post seismic movement of Mizusawa after the 2011 off the Pacific coast of Tohoku Earthquake continues. The position and velocity of Mizusawa is continuously monitored by GPS. The coordinates in Table are provisional and will be revised with accumulation of geodetic data by GPS and VLBI.

In order to maintain the antenna position accuracy, the VERA project has three kinds of geodetic observations. The first is participation in JADE (JApanese Dynamic Earth observation by VLBI) organized by GSI (Geographical Survey Institute) and IVS-T2 session in order to link the VERA coordinates to the ITRF2008 (International Terrestrial Reference Frame 2008). Basically Mizusawa station participates in JADE nearly every month. Based on the observations for four years, the three-dimensional positions and velocities of Mizusawa station till 2011 March 9 is determined with accuracies of 7 – 9 mm and about 1 mm/yr in ITRF2008 coordinate system. But the uncertainty of several centimeters exists in the position on and after 2011 March 11. The second kind of geodetic observations is monitoring of baseline vectors between VERA stations by internal geodetic VLBI observations. Geodetic positions of VERA

antennas relative to Mizusawa antenna are measured from geodetic VLBI observations every two weeks. From polygonal fitting of the six-year geodetic results, the relative positions and velocities are obtained at the precisions of 1-2 mm and 0.8-1 mm/yr till 2011 March 10. The third kind is continuous GPS observations at the VERA sites for interpolating VLBI geodetic positions. Daily positions can be determined from 24 hour GPS data. The GPS observations are also used to estimate tropospheric zenith delay of each VERA site routinely. The time resolution of delay estimates is 5 minutes.

2.8.2 Brief Summary of KVN Geodetic Measurement

KVN antenna positions are regularly monitored using GPS and geodetic VLBI observations. The K-band geodesy VLBI program between KVN and VERA has been started in 2011. Current KVN antenna positions (see Figure 15) are obtained from the KaVA K-band geodesy on 2014 January 24. The typical 1-sigma errors of geodetic solutions are about 0.4 cm in X, Y, and Z directions. Based on 22-epoch KaVA K-band geodetic observations from September 2012 to December 2016, uncertainty of KVN antenna positions are ~ 2.38 cm at Yonsei, ~ 2.55 cm at Ulsan and ~ 1.58 cm at Tamna.

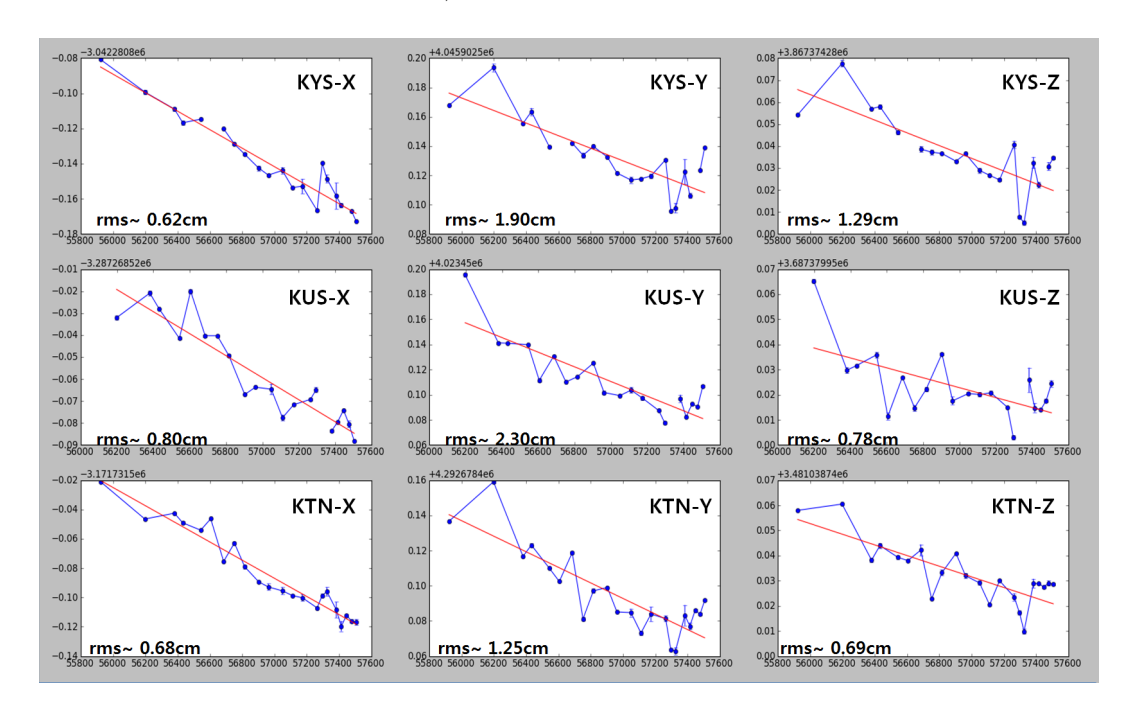


Figure 15: The trend of KVN antenna positions (IVP) in ITRF2014 coordinate system. The x and y axes are MJD and X/Y/Z in meter. The linear fitted is applied to the measurements, shown as red line, and its deviation is also presented in each axis as "rms".

3 Observing Proposal

3.1 Call for Proposals (CfP)

We invite proposals for the open-use observations of EAVN. Please refer to the following EAVN webpages for more details about the array and its performance, and how to prepare and submit a proposal.

This EAVN open-use call is based on risk-share, and provides opportunities of VLBI observations at 22 and 43 GHz for astronomers in the world. If proposers are not familiar with EAVN, they are recommended to include at least one collaborator from EAVN. The contact address for the support is eavnhelp(at mark)kasi.re.kr.

EAVN observations are conducted with single polarization (LHCP) and the data are recorded with the data rate of 1 Gbps. The data obtained at NRO45 and TAK32 are recorded with the data rate of 2 Gbps and reformatted to 1 Gbps data at Mizusawa VLBI Observatory of NAOJ. The total observation time for EAVN is up to 500 hours, while the available observing time for each EAVN telescope is different between each other, as shown in Table 9.

Table 9: Available observing time and frequency for each EAVN telescope.

		1 ··· · J		<u>-</u> -
Array/telescope	Total time [h]	Max. request time	Frequ	ıency
		for one proposal [h]	22 GHz	43 GHz
KaVA	500	150	•	•
Tianma (TMRT65)	200	60	•	•
Nanshan (NSRT26)	150	60	•	
Nobeyama (NRO45)	36	24	•	•
Takahagi (TAK32)	50	24	•	

Special conditions to be considered for EAVN proposal submission are shown below.

- Total telescope time for KaVA is 500 hours, and proposers can request for the maximum total observation time of 150 hours for one proposal. Note that KaVA is a mandatory array for all EAVN observations.
- Total telescope time for TMRT65 and NSRT26 is 200 hours and 150 hours, respectively, and proposers can request for the maximum total observation time of 60 hours for each telescope for one proposal.
- Total telescope time for NRO45 is 36 hours, and proposers can request for the maximum total observation time of 24 hours for one proposal. Please include 1-hour additional time for overhead to each observing epoch in NRO45's total request time if your proposal requires NRO45 to join. If your proposal consists of two-epoch observations with the observing time of 8 hours per epoch with NRO45, for example, total request time for NRO45 shall be 18 hours (= (8+1) hours ×2 epochs). Available date for EAVN observations with NRO45 is fixed from 2019 April 21 through 24, except April 23, 00:00 08:00 UT for system maintenance. Moreover, NRO45's

telescope time is allocated to the slots of consecutive 12 hours (00:00 - 12:00 UT or 12:00 - 24:00 UT) or 24 hours (00:00 - 24:00 UT or 12:00 - 12:00 (+ 1 day) UT).

- In the 2020A semester, EAVN accepts a request of usage of sub-array configuration (KaVA 7 telescopes and additional telescopes from NRO45, TMRT65, NSRT26, and TAK32), as well as EAVN full array configuration with 11 or 9 telescopes at 22 or 43 GHz, respectively. A proposer shall clarify the reason for the choice of sub-array configuration in the proposal.
- EAVN observations will be scheduled between 11th January 2020 and 10th June 2020, while NRO45 will be able to participate in EAVN observations until the beginning of May 2020 due to availability of the telescope.

In summary, non-KaVA telescopes (TMRT65, NSRT26, NRO45, and TAK32) will participate in EAVN observations together with KaVA according to scientific needs and their availability. Note that proposals submitted to EAVN can be assigned to KaVA according to the decision by the EAVN Time Allocation Committee (TAC).

EAVN proposal submission deadline is at

08:00 UT on 15th November, 2019.

Detailed information on the EAVN call-for-proposal can be found in the following webpage:

https://radio.kasi.re.kr/eavn/proposal_info.php

3.2 Proposal Submission

The EAVN proposal application form and proposal submission are available at the EAVN website. If you have any questions regarding to your proposal submission, contact to "eavnprop(at mark)kasi.re.kr". A proposal shall contain the coversheet (two pages), scientific and technical justification including figures and tables (maximum of three pages) with the minimum font size of 10 points. The results of the review will be announced to each PI in early January, 2020.

3.3 Special Condition for Selecting Proposals

All submitted proposals for EAVN are reviewed by referees and the EAVN TAC allocates the observing time based on the referee's rating. A proposal submitted for EAVN observations could be allocated as KaVA observations depending on its rating and the decision made by TAC. Proposers thus should specify the necessity of including non-KaVA telescopes in your observations.

3.4 Observation Mode

EAVN provides opportunities of observations at two observing frequencies, 22 and 43 GHz. All EAVN observations are conducted with single polarization (LHCP) and with the data recording rate of 1 Gbps (total bandwidth of 256 MHz). Three types of

setup of the digital filter ('C2 mode' with 2 IFs \times 128 MHz, 'C4 mode' with 8 IFs \times 32 MHz, and 'C5 mode' with 16 IF \times 16 MHz) are available, while the C2 mode is not available if your proposal contains requests for usage of non-KaVA stations. The C4 mode is available at both frequencies, while the C5 mode can be used at only 22 GHz. Available observing mode of EAVN is summarized in Tables 10 and 11. Note also that an observation at 43 GHz is available until the middle of May 2020 if NRO45 is included in your EAVN observations. This is due to the availability of NRO45, as mentioned in Section 3.1.

Table 10: Available observing mode of EAVN.

		<u> </u>
Frequency	$22~\mathrm{GHz}$	43 GHz
Telescope	KaVA, NRO45, TMRT65,	KaVA, NRO45, TMRT65
	NSRT26, TAK32	(9 telescopes)
	(11 telescopes)	
Backend mode	$C2^a$, $C4$, $C5$	$C2^{a}, C4, C5^{b}$
Recording rate		1 Gbps^c
Polarization	Left-hand circu	lar polarization (LHCP)
Correlator	Daejeon H	ardware Correlator

^a C2 mode is available at only KaVA 7 telescopes.

Table 11: Available observing mode for each EAVN telescope.

Telescope	Frequency			Observing mode				
	22 GHz	43 GHz	Total int. ^a	Fast sw. ^b	Astrometry c	HB^c	$\overline{\mathrm{WFI}^d}$	
KaVA	•	•	•	•	•	•	•	
TMRT65	•	•	•	$ullet^f$				
NSRT26	•		•					
NRO45	•	•	•					
TAK32	•		•					

^a Total intensity imaging.

3.5 Possible Conflict/Duplication with KaVA/EAVN Large Programs

In order to avoid conflict and/or duplication of the targets with existing KaVA Large Programs (LPs), proposers are highly recommended to visit the KaVA LP webpage where KaVA LPs and their source lists are presented:

https://radio.kasi.re.kr/kava/large_programs.php.

 $[^]b$ C5 mode is available at KaVA and TMRT65.

 $[^]c$ The data obtained at NRO45 and TAK32 are recorded with 2 Gbps and reprocessed to 1 Gbps.

 $[^]b$ Fast antenna switching. See Section 4.1.

^c Astrometry mode. See Section 4.1.

^d 1-beam hybrid mode. See Section 4.2.

^e Wide-field imaging. See Section 4.3.

 $[^]f$ The mode is available at only 22 GHz.

Proposals to be submitted for this opportunity should not have the same scientific goal with LPs, while it is fine to propose same sources with LPs if your proposal has a different scientific goal with LPs.

3.6 Target of Opportunity (ToO) Observations

EAVN accepts ToO proposals. Proposers can request the participation of TMRT65 and NSRT26 as well as KaVA for ToO observations, while both telescopes will join only on a best effort basis. Note that both NRO45 and TAK32 cannot be included for ToO proposals.

It is strongly recommended that ToO proposals (especially expected ToO) are submitted during the regular CfP. Unexpected or urgent ToO can be submitted as Director's Discretionary Time (DDT) proposals. ToO proposals must include clear triggering criteria to initiate an observation. ToOs are valid for one year after it is approved. ToO proposals for DDT should follow the same format of regular call and should be sent to "eavnprop(at mark)kasi.re.kr".

3.7 Angular Resolution and Largest Detectable Angular Scale

The maximum angular resolution for EAVN observations is 0.55 mas at 22 GHz for VERA-Ogasawara – NSRT26 baseline, and 0.63 mas at Q-band for VERA-Mizusawa – VERA-Ishigakijima baseline. The synthesized beam size strongly depends on UV coverage, and could be higher than the values mentioned above because the baselines projected on UV plane become shorter than the distance between telescopes. The beam size can be calculated approximately by the following formula;

$$\theta \sim 2063 \left(\frac{\lambda}{[\text{cm}]}\right) \left(\frac{B}{[\text{km}]}\right)^{-1} [\text{mas}],$$
 (2)

where λ and B are observed wavelength in centimeter and the maximum baseline length in kilometer, respectively.

The minimum detectable angular scale for interferometers can be also expressed by equation (2), where the baseline length B is replaced with the shortest one among the array. Because of the relatively short baselines provided by KVN, ~ 300 km, KaVA is able to detect an extended structure up to 9 mas and 5 mas for the K- and Q-bands, respectively.

As for an EAVN array in which non-KaVA stations (except NSRT26) are added to KaVA, the longest/shortest baselines remain the same as those of KaVA The maximum angular resolutions and the largest detectable angular scales are thus basically the same, although their detailed values in a synthesized image are dependent on the scheme of UV weighting as well as the UV coverage. As for an EAVN array which additionally includes NSRT26 at K-band, the longest baseline length extends to 5100 km (primarily along the east-west direction). This enhances the maximum angular resolution at K-band by a factor of ~ 2.2 compared to that of KaVA.

3.8 Sensitivity

When a target source is observed, a noise level $\sigma_{\rm bl}$ for each baseline can be expressed as

$$\sigma_{\rm bl} = \frac{2k}{\eta} \frac{\sqrt{T_{\rm sys,1} T_{\rm sys,2}}}{\sqrt{A_{e1} A_{e2}} \sqrt{2B\tau}} = \frac{1}{\eta} \frac{\sqrt{SEFD_{\rm sys,1} SEFD_{\rm sys,2}}}{\sqrt{2B\tau}},\tag{3}$$

where k is Boltzmann constant, η is quantization efficiency (~ 0.88), $T_{\rm sys}$ is system noise temperature, SEFD is system equivalent flux density, A_e is antenna effective aperture area ($A_e = \pi \eta_A D^2/4$ in which A_e and D are the aperture efficiency and antenna diameter, respectively), B is the bandwidth, and τ is on-source integration time. Note that for an integration time beyond 3 minutes (in the K-band), the noise level expected by equation (3) cannot be attained because of the coherence loss due to the atmospheric fluctuation. Thus, for finding fringe within a coherence time, the integration time τ cannot be longer than 3 minutes. For VLBI observations, signal-to-noise ratio (S/N) of at least 5 and usually 7 is generally required for finding fringes.

A resultant image noise level $\sigma_{\rm im}$ can be expressed as

$$\sigma_{\rm im} = \frac{1}{\sqrt{\Sigma \sigma_{\rm bl}^{-2}}}. (4)$$

If the array consists of identical antennas, an image noise levels can be expressed as

$$\sigma_{\rm bl} = \frac{2k}{\eta} \frac{T_{\rm sys}}{A_e \sqrt{N(N-1)B\tau}} = \frac{1}{\eta} \frac{SEFD}{\sqrt{N(N-1)B\tau}},\tag{5}$$

where N is the number of antennas. Using the typical parameters shown in Table 12, baseline and image sensitivity values of EAVN can be calculated as listed in Tables 13 and 14 (baseline and image sensitivities of KVN, VERA, and KaVA, as well as EAVN, are also shown for reference). Table 13 contains all combinations of baselines, while Table 14 indicates part of possible combinations of telescopes.

Station K-band Q-band $T_{\rm sys}$ [K] SEFD [Jy] $T_{\rm sys}$ [K SEFD [Jy] η_{A} η_{A} **KVN** 1992 100 0.6 1328 150 0.6 120 250 4395VERA 0.52110 0.5TMRT65 60 0.566 0.5100 110 NSRT26 42 0.6 364 NRO45 100 0.612852000.53655 TAK32 40 460 0.4

Table 12: Parameters of each telescope.

Figures 16 and 17 show the system noise temperature at Mizusawa and Ulsan, respectively. For Mizusawa, receiver noise temperatures are also plotted.

Note that the receiver temperature of VERA includes the temperature increase due to the feedome loss and the spill-over effect. In Mizusawa, typical system temperature in the K-band is $T_{\rm sys}=150$ K in fine weather of winter season, but sometimes rises

Table 13: Baseline sensitivity of EAVN.

		K-band						Q-1	band	
	KVN	VERA	TM65	NRO45	NS26	TAK32	KVN	VERA	TM65	NRO45
KVN	6.1	7.7	1.7	2.8	3.2	3.6	9.1	13.6	2.2	5.2
VERA	_	9.7	2.1	3.6	4.1	4.5	_	20.2	3.2	7.8
TMRT65	_	_	_	0.8	0.9	1.0	_	_	_	1.2
NRO45	_	_	_	_	1.5	1.7	_	_	_	_
NSRT26	_	_	_	_	_	1.9	_	_	_	_

Note: 1σ baseline sensitivity values are listed in unit of mJy, which assume an integration time of 120 seconds and a bandwidth of 256 MHz for the calculation. In the case of narrower bandwidth of 15.625 KHz (for maser emission), sensitivities can be calculated by multiplying a factor of 128.

Table 14: Image sensitivity of EAVN.

Array	$N_{\rm ant}$	$N_{\rm bl}$	K-band	Q-band
KVN	3	3	320	480
VERA	4	6	360	750
KaVA	7	21	160	285
KaVA+TMRT65	8	28	95	165
KaVA+NRO45	8	28	110	205
KaVA+TMRT65+NRO45	9	36	70	125
KaVA+TMRT65+NSRT26	9	36	75	_
KaVA+TMRT65+NSRT26+NRO45	10	45	60	_
KaVA + TMRT65 + NSRT26 + NRO45 + TAK32	11	55	50	_

Note: $N_{\rm ant}$ and $N_{\rm bl}$ are the numbers of telescopes and baselines for each array. 1σ image sensitivity values are listed in unit of μ Jy, which assume an integration time of 4 hours and a total bandwidth of 256 MHz for the calculation. In the case of narrower bandwidth of 15.625 kHz (for maser emission), sensitivities can be calculated by multiplying a factor of 128.

above $T_{\rm sys}=300$ K in summer season. The system temperature at Iriki station shows a similar tendency to that in Mizusawa. In Ogasawara and Ishigakijima, typical system temperature is similar to that for summer in Mizusawa site, with typical optical depth of $\tau_0=0.2\sim0.3$. The typical system temperature in the Q-band in Mizusawa is $T_{\rm sys}=250$ K in fine weather of winter season, and $T_{\rm sys}=300-400$ K in summer season. The typical system temperature in Ogasawara and Ishigakijima in the Q-band is larger than that in Mizusawa also.

The typical system temperature in the K-band at all KVN stations is around 100 K in winter season. In summer season, it increases up to ~ 300 K. In the Q-band, the typical system temperature is around 150 K in winter season and 250 K in summer season at Yonsei and Tamna. The system temperature of Ulsan in the Q-band is about 40 K lower than the other two KVN stations. This is mainly due to the difference in receiver noise temperature (see Table 5).

3.9 Calibrator Information

The NRAO VLBA calibrator survey is very useful to search for a continuum source which can be used as a reference source to carry out the delay, bandpass, and phase calibrations. The source list of this calibrator survey can be found at the following

VLBA homepage,

http://www.vlba.nrao.edu/astro/calib/index.shtml.

For delay calibrations and bandpass calibrations, calibrators with 1 Jy or brighter are strongly recommended as listed in the VLBA fringe finder survey:

http://www.aoc.nrao.edu/~analysts/vlba/ffs.html.

Interval of observing calibrator scans must be shorter than 1 hour to track the delay and delay rate in the correlation process.

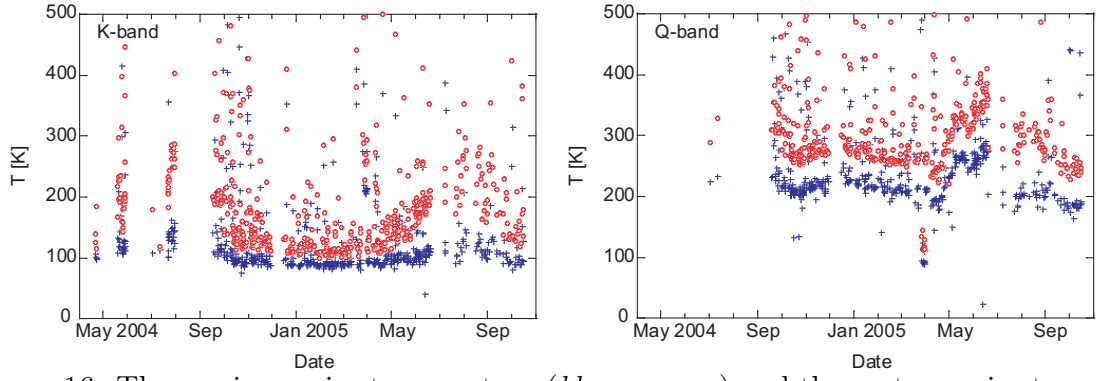


Figure 16: The receiver noise temperature (*blue crosses*) and the system noise temperature (*red open circles*) at the zenith at K-band (left) and Q-band (right) in VERA-Mizusawa station.

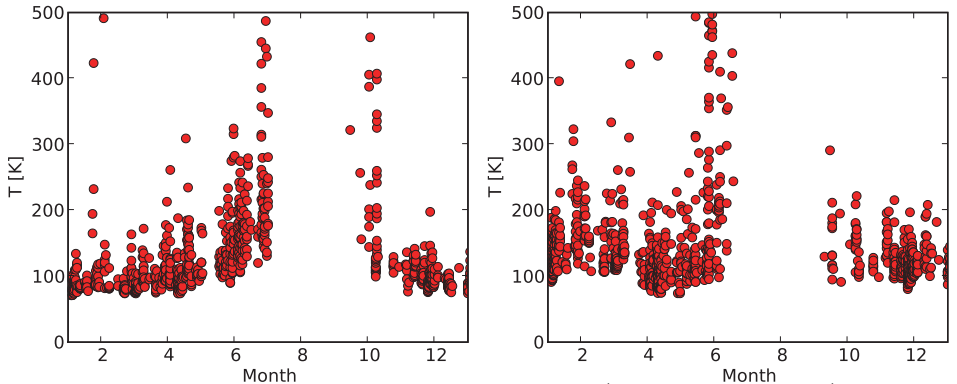


Figure 17: The zenith system noise temperature (red filled circles) at K-band (left) and Q-band (right) in KVN-Ulsan station.

3.10 Data Archive

The users who proposed the observations will have an exclusive access the data for 18 months after the correlation. After that period, all data for EAVN open-use observations will be released as archive data. Thereafter, archived data will be available to any user upon request. This policy is applied to each observation, even if the proposed observation is comprised of multi-epoch observations in this season.

4 Notes for special modes

In this section, we summarize additional information about special observing/data analysis modes.

4.1 Phase-referencing and astrometry

EAVN is capable of phase-referencing observations to image weak target sources, which cannot be detected within coherent time, and to conduct absolute astrometry measurements. Note that the array performance of this mode has been confirmed for the K-band observations with KaVA 7 telescopes. Although we do not prevent EAVN proposers from submitting proposals with the phase-referencing mode at Q-band and/or with the mode using non-KaVA telescopes within the maximum driving speed of each antenna shown in Table 3, the data quality is not guaranteed.

4.1.1 VERA dual-beam and KVN single-beam observations

In an astrometric observation, the observation using dual-beam for VERA and single-beam for KVN is recommended. KVN uses the conventional fast antenna-switching (or nodding) mode for VLBI phase reference observations. In this mode, the antenna is nodding between the bright phase calibrator and target source. By fringe fitting of the phase calibrator, the residual phase from the unmodeled clock and atmosphere can be dertermined and then interpolated to the target source to achieve a stable phase of the target source. With this mode, we can detect and image weak sources, which can not be imaged directly by fringe fitting. Regarding antenna switching cycle for the fast antenna nodding with KVN, users can refer to Table 17.

VERA employs the dual-beam observation mode. Note that VERA dual-beam system can observe two adjacent objects only with a separation angle between 0.32 and 2.2 degrees at K-band (0.32 and 2.18 for Q-band). Also, it is strongly recommended to observe pair sources with small separation angle (e.g., less than 1 degree) at high elevation (see Table 16). This will reduce the position errors caused by the residuals in atmospheric zenith delay. Note that Table 16 could be used to estimate accuracies of relative astrometry for VERA and KaVA, since the maximum baselines of both arrays are consistent with each other (i.e. positional accuracy of relative astrometry can be given by $\sim \theta_{\rm sep} \frac{c\Delta\tau}{|B|}$ where $\theta_{\rm sep}$ is the separation angle between target and phase reference sources, c is the speed of light, |B| is the baseline length and $\Delta\tau$ is the uncertainty in a delay measurement, see Reid & Honma 2014).

4.1.2 Tropospheric calibration with GPS and JMA data

Generally, residual atmospheric delay errors dominate cm-wave VLBI positional accuracy. Atmospheric (tropospheric) calibration for VERA is conducted with GPS data, while that for KVN is conducted with Japan Meteorological Agency (JMA) meso-scale analysis data (Hobiger et al. 2008; JMA 2013¹). Nagayama et al. (2015, PASJ, 67, 65)

¹http://www.jma.go.jp/jma/jma-eng/jma-center/nwp/outline2013-nwp/pdf/outline2013_all.pdf

demonstrated that an error of tropospheric zenith delay $(c\Delta\tau_{\rm trop})$ can be suppressed within ~ 2 cm with both GPS and JMA data.

4.1.3 Delay recalculation table for precise position measurement

The initial delay tracking model at the KJCC correlator is not sufficient for high precision position measurement. Therefore, we provide a calibration table (called as the delay re-calculation table) to PIs, where the necessary information such as a precise geodetic model, the most-updated Earth-rotation parameters, tropospheric and ionospheric delays is included. The table can be loaded with the AIPS task "TBIN".

For this the delivery of data and calibration table will take about three months after the observation.

4.1.4 Digital filter mode

In the relative astrometric observation with KaVA, digital filter mode of "VERA1" (see Table 7) can be used in the case of pair observation of continuum sources (same as Fig. 18). Digital filter mode of "VERA7" or "VERA7MM" (see Table 7) can be used in the case of pair observation of line (e.g. H₂O maser) and continuum sources.

4.1.5 Data reduction

Generally, users are encouraged to carry out data reduction in consultation with contact person and/or support scientist in the KaVA project group. Procedure of astrometric data reduction for VERA data has been summarized in previous papers (e.g. Fig. 11 of Kurayama et al. 2011; Fig. 5 of Imai et al. 2012). Basically, the procedure of data reduction for KaVA data is consistent with that for VERA data, expect for some points.

For instance, parallactic angle should be corrected for KVN array (e.g. with the NRAO AIPS task "CLCOR" combined with the OPCODE = "PANG"), while no need to calibrate the parallactic angle for VERA array (field rotator is equipped in the VERA array).

Since KVN should be operated by fast antenna nodding mode, antenna scan difference between KVN and VERA should be cared in data reduction. For the data reduction, a flag file is generated based on an antenna log and is provided to an observation PI. The AIPS task "UVFLG" can be used to load the flag file.

4.1.6 Astrometric accuracy for KaVA K-band observations

We have confirmed that relative astrometric observation with KaVA can satisfy an expected parallax accuracy, where K-band (22 GHz) data sets were used for the evaluation (see Figures 19 and 20, and Table 18)².

As shown in Table 18, an astrometric positional error in right ascension is ~ 50 micro-arcseconds (μ as), which is consistent with a theoretical expectation, shown by Table

²We cannot guarantee the absolute position accuracy with KaVA in 2019B season, since it's under evaluation and potentially it might have a systematic positional offset with an order of 0.2 mas. Note that "capability of relative astrometry" can be guaranteed in 2020A.

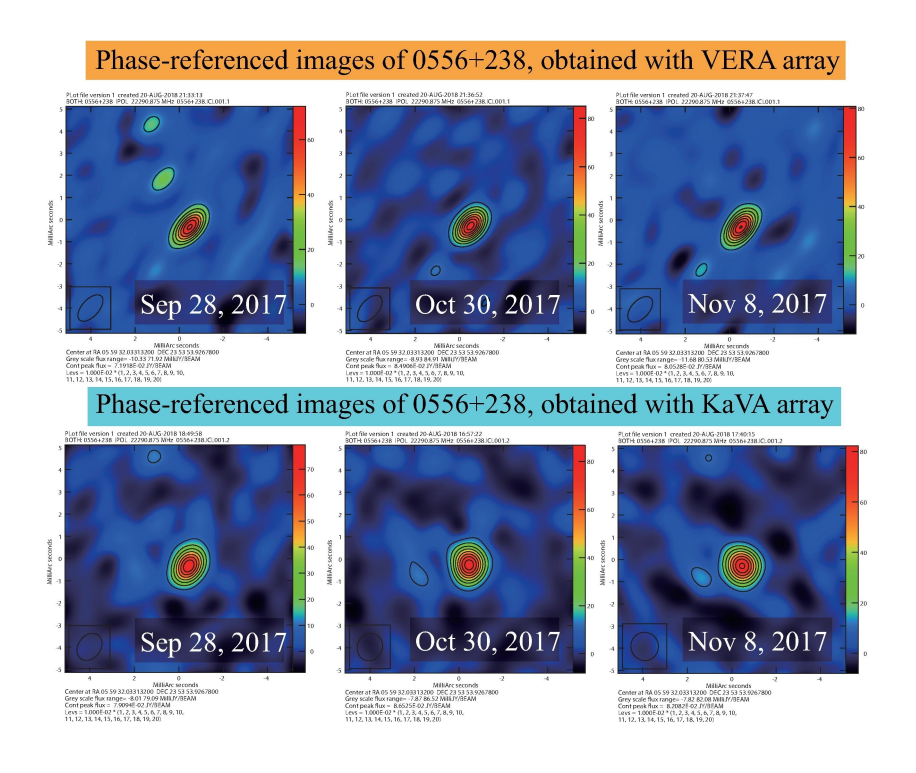


Figure 18: (**Top row**) Phase-referenced images of 0556+238 with VERA, relative to the phase reference source 0601+245. The dates of the observations are September 28th, October 30th and November 8th in 2017 from left to right images. (**Bottom row**) Same as the top row, but for KaVA data used.

16 in case of a separation angle of ~ 2 degrees and $\sigma \sim 60^{\circ}$ (i.e. 50–60 μ as). The positional error in declination is much larger than would be expected, which has been seen in previous VLBI astrometric results and it might be caused by the tropospheric zenith delay residuals (e.g. see Honma et al. 2007).

As mentioned in 4.1.5, antenna scan difference between KVN and VERA should be cared in the data reduction because of different on-source time between KVN (fast antenna nodding) and VERA (dual-beam). An example is shown in Fig. 20 where the number of visibility points for baselines including a KVN antenna is smaller than those for baselines of VERA antennas.

Table 15: Results of position repeatability for 0556+238.

	VERA			Ka	VA
Observation date	R.A.	Decl.		R.A.	Decl.
(in 2017)	(μas)	(μas)		(μas)	(μas)
September 28th	-465 ± 15	-332 ± 16		-451 ± 15	-331 ± 15
October 30th	-494 ± 11	-283 ± 12		-462 ± 16	-258 ± 18
November 8th	-505 ± 09	-318 ± 10		-480 ± 13	-287 ± 14
Unweighted mean	-488 ± 21	-311 ± 25		-464 ± 15	-292 ± 37

Column 1 shows the date of observation. Columns 2-3 display image positions of 0556+238, obtained by the phase referencing relative to 0601+245, in right ascension and declination, respectively. Note that the image positions were measured for VERA data. The errors of the positions represent the thermal error, which is typically smaller than a systematic error in ground-based VLBI observation. Columns 4-5 are the same as the Columns 2-3, but for KaVA data used.

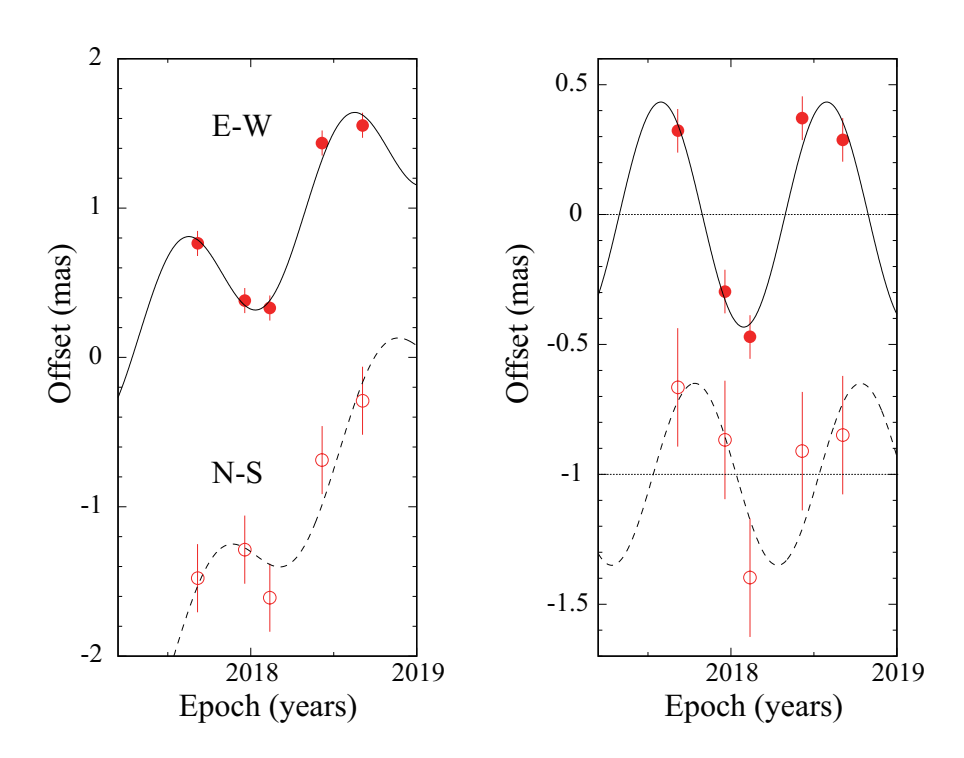


Figure 19: Results of parallax and proper-motion fitting. Plotted are position offset of maser spot (W3OH at $V_{\rm LSR} = -47.5~{\rm km~s^{-1}}$) with respect to the background QSO J0244+6228 (with a separation angle of **2.2 degrees**) toward the east (R.A.cos σ) and north (σ) as a function of time. For clarity, the north direction data is plotted offset from the east direction data. (Left) The best-fit models in the east and north directions are shown as continuous and dashed curves, respectively. (Right) Same as the Left, but with proper motions removed.

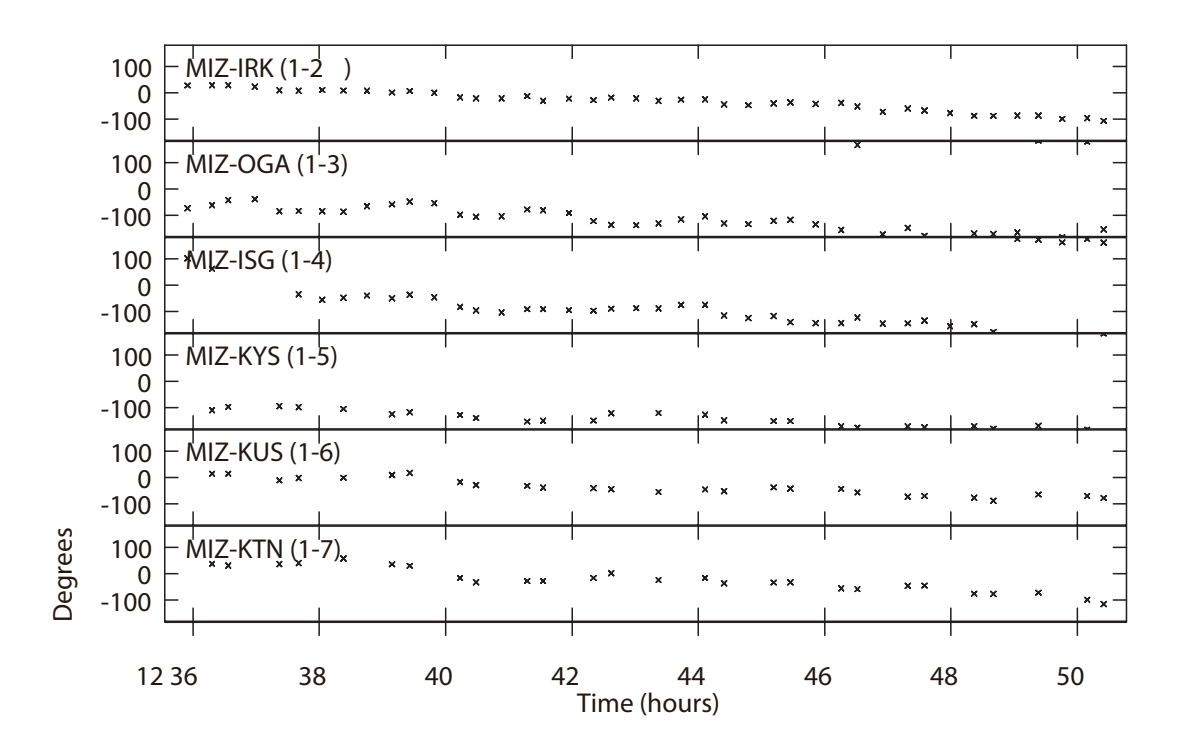


Figure 20: Points represent phase-referenced visibility phase of W3OH (at $V_{\rm LSR}=-47.5~{\rm km~s^{-1}}$) with respect to the background QSO J0244+6228 as a function of time. Each point is made with an integration time of 20 seconds. The phases for individual baselines are shown as denoted by an antenna number. The numbers indicate 1:VERA Mizusawa (MIZ); 2:VERA Iriki (IRK); 3:VERA Ogasawara (OGA); 4:VERA Ishigaki (ISG); 5:KVN Yonsei (KYS); 6:KVN Ulsan (KUS); 7:KVN Tamna (KTN).

TD.11.1C	C: 1.4:	14 C.		. C 1	*
Table Ib:	Similation	results for	accuracy	of relative	astrometry.*

		v		v
Declination	Position Angles	Separation Angles	$\sigma_{\alpha\cos\delta}$ (mas)	σ_{δ} (mas)
-30°	0°	1°	0.232	0.452
-30°	90°	1°	0.084	0.208
$+15^{\circ}$	0°	1°	0.032	0.029
$+15^{\circ}$	90°	1°	0.050	0.016
$+60^{\circ}$	0°	1°	0.030	0.018
$+60^{\circ}$	90°	1°	0.025	0.028

^{*} Referring to Honma, Tamura & Reid (2008).

Column 1 shows declination of a target source. Columns 2-3 give the position angles east of north of a background (phase reference) source relative to a target source and the separation angles between them. Columns 4-5 list positional errors in right ascension and declination, respectively. Note that the residual in atmospheric zenith delay is assumed to be 2 cm. The error of 2 cm is a typical error in the zenith delay measurements for VERA. The positional errors can be scaled by a separation angle in degrees.

4.2 1-beam hybrid (K/Q/W) mode

KaVA will enable us to conduct VLBI observations in combinations of different types of antennas (antenna beams), receiving bands, recording rates (namely total band widths), and filtered base band channels in one observing session, whose cross correlation is still valid for the whole or some parts of KaVA. In such "hybrid" observing modes with KaVA, there are some modes that are available in the 2019B CfP described as follows.

Although VERA shall use only one of dual beams in a single frequency band (K or Q), the KVN is able to observe in two to three of K/Q/W bands simultaneously in a common observing session. Please check the KVN status report for W-band information (http://radio.kasi.re.kr/kvn/status_report_2019). Signal correlation for all the KaVA baselines is valid for the band in which both the KVN and VERA observe, while that for all the observed bands is valid for the KVN baselines.

Frequency allocations should be made separately to the KVN and VERA, including base band channels that are common between the two arrays in a specific band (K or Q). Note that the number of base band channels or the total bandwidth available per frequency band is limited, therefore brighter continuum sources should be selected for group-delay calibration.

Moreover, different frequency-band assignment (K or Q) is also available for each of VERA stations to observe in K/Q-bands simultaneously. In this case, it is necessary to confirm that uv-coverages in both bands are suitable for a target source. For example, suppose a simultaneous observation of faint 44 GHz methanol maser and compact 22 GHz water masers. In this case, VERA Iriki station is assigned to a Q-band observation while other VERA stations are assigned to K-band in addition to a simultaneous K/Q-band observation with the KVN. The Q-band array becomes a compact array consisted with KVN three + VERA Iriki stations, while the K-band array becomes an extended array consisted with KVN three + VERA Mizusawa/Ogasawara/Ishigakijima stations.

4.3 Wide-field imaging mode

This mode is required to fully image 44 GHz methanol maser emissions associated with star-forming regions, which are generally distributed on the angular scale over 10 arcsec.

Table 17: Phase-Referencing Cycle Times (min).*

				J 0	\ /	
	Typic	Typical weather		weather	Good	weather
	$(C_n^{\dagger} = 1)$	$2 \times 10^7 \text{ m}^{-1/3}$	$(C_n^{\dagger} = 4)$	$4 \times 10^7 \text{ m}^{-1/3}$	$(C_n^{\dagger} = 1 \times 10^7 \text{ m}^{-1/3})$	
	Frequ	ency (GHz)	Freque	ency (GHz)	Freque	ncy (GHz)
EL (deg)	22	$(43)^{\ddagger}$	22	$(43)^{\ddagger}$	22	$(43)^{\ddagger}$
5	0.3	0.2	0.2	0.1	0.8	0.4
10	0.5	0.3	0.2	0.1	0.8	0.6
15	0.7	0.3	0.3	0.1	1.5	0.7
20	0.8	0.4	0.3	0.2	1.8	0.9
25	0.9	0.4	0.4	0.2	2.0	1.0
30	1.0	0.5	0.4	0.2	2.8	1.1
40	1.1	0.5	0.5	0.2	5.8	1.3
50	1.3	0.6	0.6	0.3	9.9	1.5
60	1.8	0.7	0.6	0.3	10.0	2.2
70	2.3	0.7	0.6	0.3	10.0	2.9
80	2.6	0.7	0.6	0.3	10.0	3.3

^{*} Referring to Ulvestad, J., Phase-Referencing Cycle Times, VLBA Scientific Memo 20 (1999).

Column 1 shows antenna elevation angles. Columns 2-3 indicate phase-referencing cycles at 22 and 43 GHz, respectively, under typical weather condition. The phase-referencing cycle is defined as the time between the midpoints of the two calibrator observations before and after the target observation. Columns 4-5 are the same as Columns 2-3, but with bad weather condition (similar to some summer days). Columns 6-7 are the same as Columns 2-3, but with good weather condition (similar to some winter nights).

Table 18: Parallax results for W3OH*.

Array	Frequency	Source	$V_{ m LSR}$	Parallax	$\sigma_{lpha{ m cos}\delta}^*$	$\sigma_{\delta}{}^*$	Ref.
	GHz		${\rm km~s^{-1}}$	(mas)	(mas)	(mas)	
KaVA	22	W3OH	-47.5	$0.460 {\pm} 0.035$	0.052	0.256	
VLBA	22	W3OH	$-51.5 \sim -48.2$	$0.489 {\pm} 0.017$	$\sim \! 0.050$	~ 0.050	(1)

^{*}Positional errors in right ascension and declination were adjusted so that the reduced chi-square becomes unity. Bright and compact maser spot was used for the parallax fit.

Columns 1-2 represent array and observing frequency. Columns 3-4 show source name and LSR velocity of the maser spot, used for the parallax fit. Column 5 displays the parallax result of the source in milli-arcseconds (mas). Columns 6-7 represent the (systematic) positional errors in right ascension and declination, respectively.

Ref. (1) Hachisuka et al. (2006).

The wide-field imaging (WFI) mode is achieved with an accumulation period shorter than the usual one of 1.6384 sec in Daejeon correlator at KJCC. Theoretically, the field of view (FoV) within an amplitude loss of 1%, 5%, and 10% is estimated on the basis of the time-average smearing effect due to a finite accumulation period [?]. The FoVs calculated for accumulation periods of 0.2048, 1.6384, and 3.2768 sec are summarized in Table 19, in the case of the highest angular resolution at Q-band of 0.6 mas with KaVA.

In the current available specification of Daejeon correlator, there is a trade-off between a shorter accumulation period and a larger number of IF channels to yield higher spectral resolution. The most highly recommended setup is the combination of C2 mode and an accumulation period of 0.2048 sec, in which both a sufficiently high velocity resolution (0.11 km s⁻¹ for 44 GHz methanol masers) and a sufficiently wide FoV (10 arcsec or more) can be obtained. Thus the recommended set-up for WFI mode is summarized in Table 20.

^{\dagger} C_n is strength of the tropospheric turbulence.

[‡] Now, Q-band phase-referencing mode is not opened.

Table 19: FoV within a given amplitude loss in each accumulation period*.

Accumulation	Amplitude loss				
period	1.0%	5.0%	10.0%		
(sec)	(arcsec)	(arcsec)	(arcsec)		
0.2048	8.6	19.4	27.4		
1.6384	1.1	2.4	3.4		
3.2768	0.5	1.2	1.7		

^{*} Under an assumption of the highest angular resolution at Q-band of 0.6 mas with KaVA.

Table 20: Recommended set-up for WFI mode in the current situation.

Correlation	Sampling	Bandwidth	Accumulation	Spectral
mode	rate	$/\mathrm{IF}$	period	channels/IF
C2	$1024 \; \mathrm{Mbps}$	128 MHz	$0.2048 \sec$	8,192

The evaluation for the WFI tests was done by the following two ways: comparing the data of an accumulation period of 0.1 sec produced in DiFX to those of 0.2048 sec in Daejeon correlator, and comparing the latter data to the same data but with averaging in 3.2768 sec. These ways provide us a chance to estimate whether such an isolated maser can be detected or not and how much rate of the amplitude loss occurs. The evaluation might be updated on the basis of a comparison between a short-accumulation period data and a multi-tracking center data in the near future.

If you would like to require this WFI mode, please describe your requests in the following two items:

- Requested setting parameters for WFI in the proposal cover sheet
- Reasons for requiring WFI mode in the scientific justification

Finally, note that the file size of correlated data for WFI is as huge as \sim 600 GByte. We therefore recommend to check and improve the performance of your internet environment and personal computer as high as possible for comfortable data downloading and data processing, respectively. Please refer an example parameters in Table 21:

Table 21: Required performances of internet and personal computer.

Forward speed	$\geq 10 \; \mathrm{MByte \; s^{-1}}$
HDD/SSD volume	$\geq 1.5 \text{ TByte}$
RAM	\geq 16 GByte

Here, the experiment to verify the time-average smearing effect due to a finite accumulation period has been done, however we will also verify the bandwidth smearing effect to KaVA observations in the near future.

5 Observation and Data Reduction

5.1 Preparation of an EAVN Observation

After the acceptance of proposals, users are requested to prepare the observing schedule file two weeks before the observation date. The observer is encouraged to consult a contact person in the EAVN Array Operation Center (AOC) and/or the assigned support scientist to prepare the schedule file under the support of the contact person and/or the assigned support scientist. The schedule submission should be done by a stand-alone vex file. The examples of EAVN vex file are available at the EAVN web site:

http://radio.kasi.re.kr/kava/kava_observing_preparation.php

Detailed information about preparation and submission of a schedule file for TMRT65 and NRO45 will be announced when distributing the proposal review results.

On your schedule, we strongly recommend to include at least two fringe finder scans, each lasting 5 or more minutes at the first and latter part of observation in order to search the delay and rate offsets for the correlation.

For EAVN which includes the large telescopes (TMRT65 and NRO45), regular pointing check is necessary at both 22 and 43 GHz. You should leave a 8-15 min gap every $\leq 1-2$ hr in your schedule file to allow this. Pointing check is done by the local operators. In addition, we strongly recommend to include frequent scans of a maser source and/or a bright compact continuum source located within 15° from the target. This allows a cross check of the amplitude calibration for TMRT65 and NRO45 along with the usual a priori method.

We request PIs to specify their correlation parameters at the beginning of the vex file for proper correlation processing. In particular, PIs who request for sub-array or dual-beam observations for EAVN should provide a frequency matching table for the correct correlation.

5.2 Observation and Correlation

EAVN members take full responsibility for observation and correlation process, and thus basically proposers will not be asked to take part in observations or correlations. Observations are proceeded by operators from each array and telescope, and correlated data is delivered to the users in approximately two months including the time for media shipping to KJCC at Daejeon.

After the correlation, the user will be notified where the data can be downloaded by e-mail. After one month later of a correlated data distribution to PIs, disk modules which contains raw observing data can be recycled without notice. Therefore, PIs should investigate the correlated output carefully. For re-correlation or raw data keeping of the data, PI should provide adequate evidence in order to justify his/her request. If there is an issue related to correlated data, PI should consult a support scientist first or the correlator team (kjcc (at-mark) kasi.re.kr), and not to ask KJCC members directly.

5.3 Data Reduction

For EAVN data reduction, the users are encouraged to reduce the data using the NRAO AIPS software package. The observation data and calibration data will be provided to the users in a format which AIPS can read.

As for the amplitude calibration, we will provide "ANTAB" files which include the system temperature information measured by the R-sky method and the information of the dependence of aperture efficiency on antenna elevation. If the user wants weather information, the information of the temperature, pressure, and humidity during the observation can be provided.

At present, EAVN does not support astrometric observations. In case of questions or problems, the users are encouraged to ask the contact person in EAVN members and/or the assigned support scientist for supports.

5.4 Further Information

The users can contact any staff member of EAVN by e-mail (see Table 22). Note that your EAVN proposal should be submitted to the following EAVN proposal submission site.

https://radio.kasi.re.kr/eavn/proposal_info.php

Table 22: Contact addresses.

Name	E-mail address	Related Field
Inquiry about	eavnprop (at-mark) kasi.re.kr	Proposal-related requests/questions
proposal submission		
User support team	eavnhelp (at-mark) kasi.re.kr	User support in general
Operation team	eavnobs (at-mark) kasi.re.kr	Observation-related requests/questions,
		schedule submission
Correlator team	kjcc (at-mark) kasi.re.kr	Correlation-related requests/questions,
		correlated data distribution

References

- [1] KaVA Status Report for 2019B: https://radio.kasi.re.kr/kava/status_report19b/node3.html
- [2] NRO web site: http://www.nro.nao.ac.jp/~nro45mrt/html/index-e.html
- [3] Cho, I. et al. 2017, PASJ, 69, 87
- [4] Han, S.-T., et al. 2008, Int. J. Infrared Millimeter Waves, 29, 69
- [5] Han, S.-T., et al. 2013, PASP, 125, 539
- [6] Lee, S.-S. et al. 2015, JKAS, 48, 229
- [7] Oh, S.-J., et al. 2011, PASJ, 63, 1229

- $[8] \ \, {\rm Oyama}, \, {\rm T. \, \, et \, \, al. \, \, 2016}, \, {\rm PASJ}, \, 68, \, 105$
- $[9]\,$ Yonekura, Y. et al. 2016, PASJ, 68, 74